1850

experimental muffin tin potential parameters from fermi surface data

m.a.c. devillers

EXPERIMENTAL MUFFIN TIN POTENTIAL PARAMETERS

FROM

FERMI SURFACE DATA

PROMOTOR:

PROF.DR. A.R. DE VROOMEN

EXPERIMENTAL MUFFIN TIN POTENTIAL PARAMETERS FROM FERMI SURFACE DATA

PROEFSCHRIFT

ter verkrijging van de graad van doctor in de

Wiskunde en Natuurwetenschappen aan de

Katholieke Universiteit te Nijmegen, op gezag van de

Rector Magnificus Prof. Mr. F.J.F.M. Duynstee,

volgens besluit van het college van decanen

in het openbaar te verdedigen op donderdag

9 mei 1974 des namiddags te 2 uur precies

door

MARINUS ANTONIUS CORNELIS DEVILLERS

geboren te Wouw

1974

Offsetdrukkerij van Mameren, Nijmegen

Il faut toujours bien faire ce qu'on fait, même une folie.

Honoré de Balzac

Allen, die in de afgelopen jaren, direkt of indirekt, hebben bijgedragen aan de tot stand koming van dit proefschrift, wil ik graag langs deze weg bedanken.

In het bijzonder de kritieken en de hulp van mijn collega's wil ik memoreren.

Ook dank ik dr.Q.Andersen en prof. W.H. Young voor de stimulerende discussies, die ik met hen mocht hebben.

Mevr. Nellie Snijders, mej. Riki Gommers en mrs. Muriel Parke, alsmede de medewerkers van de afdelingen Illustratie en Fotografie in de persoon van respectievelijk dhr. Gerritsen en dhr. Spruyt, bedank ik voor hun daadwerkelijke bijdragen aan de uiterlijke vormgeving van dit proefschrift.

Contents

I. Introduction 3

II. Theory. 7

II.1 General outline of APW formalism. 7

II.2 l- and K - convergence aspects. 10

II.3 Other muffin tin potential based formalisms. 12

II.4 OFS - approximation; comparison with local pseudo potential formalism. 14

II.5 Scattering theory in solid state physics; Friedel picture. 15

II.6 Lloyd picture. 17

II.7 Small energy limit of $\eta_l(E_F)$ and of $Z(E_F)$. 19

II.8 Modified t-matrix. 21

II.9 E_F-ambiguity; first order approach to the band structure problem; conservation of matrix element in first order and its consequences. 23

II.10 Second order approach to the band structure problem. 25

II.11 Relativistic RAPW scheme; spin orbit coupling. 27

II.12 (R)APW scheme for crystals with more than one atom per primitive cell. 28

III. Computational aspects of APW interpolation. 30

III.1 Least squares fit of muffin tin potential parameters to experimental points on the FS in the APW scheme. 30

III.2 Convergence aspects; size of determinant; Löwdin procedure; degenerated $\vec{k}$ points. 32

III.3 Ambiguity in the sign of Fourier transforms in first order perturbation theory. 34

III.4 Least squares fit in the relativistic APW scheme. 35

III.5 Least squares fit to d Hv A data. 36

IV. Results. 37

IV.1 White tin. 37

IV.2 The noble metals. 40

IV.3 Mercury. 42

IV.4 Experimental behaviour of a_1, η_1 and Z as a function of E_F. 48

V. Some applications of experimental FS determined muffin tin potential parameters. 52

VI. Conclusions and suggestions for further research. 54

References. 56

List of abbreviations. 59

Appendices 61

A. The Fermi surface of white tin from a RAPW interpolation. 61

B. Pseudopotential formfactor for mercury. 107

C. The Fermi surface of mercury from a APW interpolation. 115

Summary. 132

Samenvatting. 134

Curriculum Vitae 136

I. INTRODUCTION.

One of the main tasks in solid state physics is solving the problem of the motion of electrons in perfect metallic crystals. Several approaches, like L.C.A.O. and model potential formalisms, have been applied with considerable success. In principle the calculation of electronic eigenstates is a many body problem involving say 10^{24} electrons and nuclei. To make this problem manageable one has to make some assumptions and approximations :

a. Born - Oppenheimer approximation i.e. the nuclei are supposed on fixed places in $\vec{r}$ - space

b. one - electron approximation : i.e. an electron is moving in some averaged, periodic field, arising from all other electrons and nuclei.

Then we arrive at a picture where an electron is moving in a periodic crystal potential, which motion can be described by the Bloch type solution of the one electron Schroedinger equation. One way to proceed now is to approximate the crystal potential by a "muffin tin" model, i.e. the potential is assumed to be spherically symmetric inside spheres around each ion with radius say equal to half nearest neighbours distance and is assumed to be a constant (say zero) in the remaining interstitial region. This problem can be attacked by Green's function theory and, depending on the basis one chooses to expand the crystal wave function and the Green's function, one arrives at the so called KKR (Korringa and Kohn and Rostoker (1954)),

KKRZ (KKR brought into k representation by Ziman (1965)) or APW (augmented plane wave, J.Slater (1937)) formalisms. The expansion coefficients are determined by a variational procedure. The parameters, which these various formalisms have in common, are the scattering phase shifts of the individual muffin tin potentials or, equivalently, the logarithmic derivatives of the radial part of the APW wave functions at the muffin tin sphere radius. Once the phase shifts have been evaluated at an energy E one can calculate the values of the wave vector $\vec{k}$ for which $E(\vec{k})=E$ holds, i.e. the bandstructure $E(\vec{k})$ can be determined. In particular the phase shifts at the Fermi energy are constants for the Fermi surface of a metal. (see also Segall and Ham (1968)). However the accurate construction of the muffin tin potential is a hard task theoretically as well as numerically. On the other hand from many considerations one can argue that the logarithmic derivatives of the muffin tin well should be good parameters for the description of a Fermi surface.

The object of this thesis is to investigate the ability of these muffin tin parameters to describe the geometry of a Fermi surface and what kind of further information we can get from them once they have been determined experimentally. It turns out that they are excellently suited for interpolation purposes, for example the rather complicated but experimentally accurately known Fermi surface of white tin can be described to within the experimental error just by fitting as few as four phase shifts. Further it will be found that unfortunately there exists a strong ambiguity in the choice of the Fermi energy, relative to the muffin tin zero. This is both an amazing fact, because beforehand one hardly can believe that such strongly different muffin tin potentials can reproduce the same Fermi surface, as well as a disappointment, for one should like to end up with unique values of the various parameters.

The Fermi energy ambiguity causes a lot of additional phenomena like linearity of the logarithmic derivatives as a function of the Fermi energy, specific behaviour of the Friedelsum and the existence of "focus point radii", which phenomena can be understood to some extent by studying the APW matrix elements in the so called "on the Fermi sphere" approximation.

One of the main advantages of the phase shift based bandstructure calculations over plane wave methods like OPW is the natural inclusion of those cases, where narrow d-bands are lying in the broad s - p - band, as it occurs in the noble metals for example, because such a d-band is correctly described by the d-phase shift-behaviour as a function of E. So far we have not mentioned relativistic effects, which become more important for the heavier elements. For example in the case of white tin it will turn out that spin-orbit coupling should be included.

This thesis contains the following chapters. In chapter II we will give a brief review of the theoretical foundation of the APW formalism and some statements from scattering theory. Further we will discuss phenomena, related to or arising from an experimentally found E_F ambiguity, like linear behaviour of logarithmic derivatives, conservation of APW matrix element in "on the Fermi sphere" approximation, the existence of "focus point" muffin tin radii, and the variation of the Friedelsum as a function of E_F. Finally we will discuss second order effects in bandstructure problems.

In chapter III we will discuss the computerprogram we have set up for an (R)APW fit to the experimental geometry of the Fermi surface of a metal.

The results of the calculations on Sn and Hg will be reported in chapter III, where we will make use of earlier reports now enclosed as appendices A,B and C. Further we will discuss the results on the noble metals obtained by N.Coenen from a KKRZ fit.

In chapter V we give some concluding remarks and suggestions for further investigation.

II. THEORY

II.1 General outline of APW formalism.

The augmented plane wave method (APW) was formulated for the first time in 1937 by J.Slater. But due to its numerical complexity the method had to wait for the rather large computers of the last decade before becoming popular. Now its power for solving the crystal hamiltonian has been recognized by a large public. Parallel to this developement the method of Korringa (1947) and of Kohn and Rostoker (1954)(KKR) have been established, and also the $\vec{k}$-representation of it by J.Ziman (1965) (KKRZ). The relationship between APW and KKR(Z), both methods being solutions of the muffin tin model, has been studied by several workers from whomwe mention K.H. Johnson (1966), who was able to derive both methods from a Greens function formalism by using different sets of basis functions for the expansion of the wave function and of the Greens function.

In recent years several reviews concerning phase shift based models have appeared (to mention a few: T.L. Loucks, Augmented Plane Wave Method (1967), J.Ziman (1972) and Dimmock (1972) to which the interested reader is referred. In this work we will stress only some features which are of direct interest to our work, or which can be seen as additional remarks to the above mentioned reviews.

For the derivation of the APW matrix elements we will follow Ziman (1972) in his recent review mainly. For the moment we suppose a crystal with one atom per primitive cell. The muffin tin potential V_{MT} is defined as

$$V_{MT}(\vec{r}) = V_S(r) \qquad r \leq R \tag{2.1}$$

around each ion site and

$$V_{MT}(\vec{r}) = 0 \qquad r > R \tag{2.2}$$

with $\vec{r}$ restricted to the Wigner-Seitz cell. $V_S(r)$ is expected to be very similar to the atomic Hartree-Fock potential; only for the larger r there is a marked difference because of the overlap of the outer shell atomic orbitals. R is choosen somewhat arbitrarily but usually equal to half of the nearest neighbour distance; not larger than that to avoid overlap of neighbouring potential wells. Using the definition of $V_{MT}(\vec{r})$ inside each cell we obtain the periodicity condition

$$V_{MT}(\vec{r} + \vec{l}) = V_{MT}(\vec{r}) \tag{2.3}$$

with $\vec{l}$ being a lattice vector.

The crystal one electron Schroedinger equation reads (in a.u.) for the cell centred at the origin:

$$[-\nabla^2 + V_S - E]\, \psi_{\vec{k}}(\vec{r}) = 0 \qquad r < R \tag{2.4}$$

$$[-\nabla^2 \qquad - E]\, \psi_{\vec{k}}(\vec{r}) = 0 \qquad r > R \tag{2.5}$$

Because of the spherical symmetry of $V_{MT}(\vec{r})$ inside the muffin tin spheres the wave function inside the muffin tin spheres can be written as a linear combination of $R_l(r,E)Y_{lm}(\hat{r})$, where $R_l(r,E)$ is a regular solution of the radial part of the Schroedinger equation.

$$\left[r^{-2}\frac{d}{dr}(r^2\frac{d}{dr}) + E - V_S(r) - l(l+1)r^{-2}\right] R_l(r,E) = 0 \qquad (2.6)$$

and $Y_{l\ m}(\hat{r})$ is the usual spherical harmonic. An APW wave function is defined now by

$$APW_{\vec{k}}(\vec{r}) = \begin{cases} \exp(i\vec{k}.\vec{r}) = \exp(i\vec{k}.\vec{l})\exp(i\vec{k}.\vec{r}') \text{(outside spheres)} \\ \left[\sum_{lm} i^l a_{lm} R_l(r',E) Y_{lm}(\hat{r}')\right] 4\pi \exp(i\vec{k}.\vec{l}) \text{(inside l-th sphere)} \end{cases} \qquad (2.7)$$

The coefficients $a_{l\ m}$ are determined by the condition that the $APW_{\vec{k}}(\vec{r})$ should be continuous on the muffin tin spheres. Using the well known expansion

$$\exp(i\vec{k}.\vec{r}') = 4\pi\Sigma_{lm} i^l j_l(kr') Y_{lm}(\hat{r}') Y^*_{lm}(\hat{k}) \qquad (2.8)$$

we get

$$a_{lm} = 4\pi\left\{j_l(kR)/R_l(R,E)\right\} Y^*_{lm}(\hat{k}) \qquad (2.9)$$

Taking into account the periodicity of the crystal potential we can write now the total solution $\psi_{\vec{k}}$ of the one electron Schroedinger equation (2.4),(2.5) as a linear combination of APW $\vec{k} + \vec{K}_i$

$$\psi_{\vec{k}}(\vec{r}) = \sum_{\vec{K}_i} b_{\vec{k}+\vec{K}_i} APW_{\vec{k}+\vec{K}_i}(\vec{r}) \qquad (2.10)$$

where $\vec{K}_i$ are reciprocal lattice vectors. The expansion coefficients $b_{\vec{k}+\vec{K}_i}$ can be determined by a variational procedure. The discontinuity in the slope of $APW_{\vec{k}}$ on the muffin tin sphere causes some arbitrariness in the variational procedure (R.S.Leigh, 1956). Following the procedure

of Slater we get the secular APW determinant with matrix elements (in c.u.)

$$M_{ij}^{APW}(E) = (\vec{k}_i \cdot \vec{k}_j - E)\,\delta_{ij} + \Gamma_{ij}^{APW}(E) \qquad (2.12)$$

$$\Gamma_{ij}^{APW}(E) = -\frac{4\pi R^3}{\Omega_{atom}} (\vec{k}_i \cdot \vec{k}_j - E) \frac{j_1(2\pi |\vec{k}_i - \vec{k}_j| R)}{2\pi |\vec{k}_i - \vec{k}_j| R)} +$$

$$+ \frac{R}{\pi \Omega_{atom}} \sum_l (2l+1)\alpha_l(E) j_l(2\pi k_i R) j_l(2\pi k_j R) P_l(\hat{k}_i \cdot \hat{k}_j) \qquad (2.13)$$

In (2.12) and (2.13) $\vec{k}_i = \vec{k} + \vec{K}_i$; j_l denotes the spherical Bessel function; P_l is the Legendre polynomial; Ω_{atom} the atomic volume; $\alpha_l(E) = RR'_l(E,R)/R_l(E,R)$, which is dimensionless, shall be referred to as the "logarithmic derivative" for orbital quantum number l.

II.2 l-and $\vec{K}$-convergence aspects.

At this point we wish to make some comments on the convergence properties of the APW formalism both with respect to the l-sum as well as to the size of the APW matrix.

Although the set of plane waves $\{\exp(i\vec{k}_i \cdot \vec{r})\}$ is a complete one for functions defined in the unit cell, the set $\{APW_{\vec{k}_i}\}$ is overcomplete unfortunately. The continuation (2.9) of every plane wave to inside the muffin tin spheres is a rather arbitrary one thus leaving us with a set of basis functions which is overcomplete generally. As a consequence the determinant of the infinite APW matrix vanishes for all values of E. However, the method is saved by any finite truncation of the APW secular determinant. The desired $\vec{K}_i$ convergence may then be obtained by inspection of the numerical values of the matrix elements and energy values.

It can be shown (Johnson, 1966) that the APW formalism can be derived from minimizing

$$\int_{\Omega_{out}} \left| \psi_{\vec{k}} - \sum_{i=1}^{M} a_i \exp(i\vec{k}_i \cdot \vec{r}) \right|^2 d\vec{r} \qquad (2.17)$$

and taking the limit as M goes to infinity, thus proving that the APW formalism yields the most rapidly convergent plane wave expansion of the wave function outside the spheres.

The l-truncation is determined by two requirements. First we have to include all α_l which are significantly deviating from the "empty potential" value $\alpha_l^o(E) = xj_l'(x)/j_l(x), x = 2\pi R\sqrt{E}$. In practice this condition requires a l_{max} of not larger than two or three, because for the higher l the centrifugal barrier $l(l+1)/r^2$ is overwhelming already $V_S(r)$ in the metals we are dealing with. Secondly the l-sum should be large enough to satisfy the expansion (2.8) sufficiently; for most calculations $L_{max} = 10$ suffices.

The truncation of the l-sum causes a slight discontinuity in the $APW_{\vec{k}}$ at the muffin tin radius, but this has no serious consequenc es, because in a variational procedure the trial functions are not required to be continuous.

In the discussion on $\vec{K}_i$ - and l-convergence we can include some remarks on the role of the muffin tin radius. In the definition (2.1.) and (2.2.) of $V_{MT}(r)$ the quantity R is brought in somewhat arbitrary. Usually one takes the value of R half nearest neighbours distance because for this value one intuitively expects the muffin tin model to approach most closely the real potential (the model does not allow for overlapping muffin tin spheres, although recently it has been shown that no serious errors are made if R is choosen say 10% larger than the

inscribed sphere radius, (M.J.G.Lee et al (1972), O.K. Andersen (1971), M.A.C. Devillers (1972)). The maximum value of l, needed for sufficient convergence may be decreased by decreasing R, but this will increase the size of the APW determinant for it will take more plane waves to describe $\psi_{\vec{k}}$ in the interstitional region (see equation (2.17). So R can be seen as to balance the maximum value of l against the size of the APW determinant (Leigh,R.S, 1956). For this reason one may expect the bandstructure to be rather insensitive to the value of R, provided the maximum l-value and the APW determinantal size are sufficient large (of course for the value of R within certain limits, because for example decreasing R to within the last closed shell of the atom would increase the size of the APW determinant drastically, the latter becoming no longer manageable in practice).

By inspection of the APW matrix element (2.12) we see that the only place where the potential enters in the formalism, is the logarithmic derivative $\alpha_l(E,R)$. By fixing R we note that $\alpha_l(E)$ is a constant for a surface of constant energy in $\vec{k}$-space. So they can be used as adjustable parameters for a Fermi surface. It is just this idea we want to investigate in this thesis, i.e. we are seeking an answer to the questions of with how many α_l and with how many $\vec{K}_i$ we can reproduce the experimental well determined Fermi surface of a metal. Or in other words, how well does the muffin tin model work in metals ? The way we have proceeded in practice to answer those questions, will be treated in the next chapter.

II.3 Other muffin tin potential based formalisms.

There are other formalisms based on the muffin tin model like KKR and KKRZ. These can be derived using Green's function theory and without going

in details we present immediatly the resulting KKRZ matrix element (in c.u.)

$$\Gamma_{ij}^{KKRZ}(E) = \frac{R}{\pi\Omega_{atom}} \sum_{l} (2l + 1)\, \gamma_l(E) j_l(2\pi k_i R) j_l(2\pi k_j R) \cdot P_l(\hat{k}_i \cdot \hat{k}_j) \qquad (2.18)$$

with

$$\gamma_l = \alpha_l(E) - \alpha_l^0(E) \qquad (2.19)$$

We note that (2.18) has some advantages over (2.13) in that the j_1 term is lacking and in that the l-sum converges more rapidly, for we have to include now only those l for which $\alpha_l(E)$ is significantly different from $\alpha_l^0(E)$. But there are arguments (Johnson 1966; Segall and Ham, 1968; Devillers etal, 1971) that the $\vec{K}_i$ convergence is not as fast as that of APW. Another advantage of KKRZ is that the set of trial functions on which the former is based forms a complete set. This has been pointed out by Lloyd (1965). He showed that (2.18) can be obtained form a hamiltonian, in which the muffin tin potential (2.1.) and (2.2.) is replaced by a non-local l-dependent delta-function potential at the muffin-tin radius. The solutions $\psi_l(\vec{r})$ of such a well defined Hamiltonian form a complete set and thus also the expansion of $\psi_{\vec{k}}(\vec{r})$ in a plane wave representation must be unique. Once more, as mentioned above, if we restrict ourselves to a finite size of the determinant the discussion about the completeness of the set trial functions is of little importance.

II.4 OFS-approximation : comparison with local pseudo potential formalism.

We can look upon (2.13) and (2.18) as being the Fourier transforms of some local pseudo potential describing the transition of nearly free electron states $\vec{k}_i$ into $\vec{k}_j$ (OFS-approximation). In this approximation the APW (KKRZ) matrix elements are evaluated for $k_i = k_j = k_F \equiv \sqrt{E_F^o}$ (with E_F^o is the free electron value of the Fermi energy), and they become functions of the continuous variable q (in c.u.)

$$\Gamma^{APW}(q,E_F) = -\frac{4\pi R^3}{\Omega_{atom}}(k_F^2\cos(\theta_q) - E_F)j_1(2\pi qR) / 2\pi qR +$$

$$+\frac{R}{\pi\Omega_{atom}}\sum(2l+1)\alpha_l(E_F)j_l^2(2\pi k_F R)P_l(\cos(\theta_q)) \qquad (2.20)$$

For $q > 2\,k_F$ $\vec{k}_i$ and $\vec{k}_j = \vec{k}_i + \vec{q}$ are taken antiparallel and only k_i is fixed at k_F. At the values $\vec{q}_{ij} = \vec{K}_i - \vec{K}_j$ we may expect $\Gamma^{APW}(q_{ij},E_F)$ to deviate not too much from $V(q_{ij})$ of some adequate local pseudo potential for the metal being in consideration , at least so for the "most important" q_{ij} for that metal. A further discussion of this nearly free electron argument is postponed to section II.9 and also should wait the numerical results in the next chapters.

II.5 Scattering theory in solid state physics; Friedel picture.

Another point of view in bandstructure theory is to look at the muffin tin crystal as an assembly of periodically arranged scattering potential wells.

Because the potential well is spherical symmetric a description in partial waves will be suited. The scattering phase shifts $\eta_l(E)$ of a single scatterer are related to $\alpha_l(E)$ by

$$\alpha_l(E) = x \left\{ j_l'(x) - tg\eta_l(E) n_l'(x) \right\} / \left\{ j_l(x) - tg\eta_l(E) n_l(x) \right\} \qquad (2.21)$$

with $x = 2\pi R \sqrt{E}$. For any spherical symmetric potential $V(r)$ which diverges slower than r^{-2} in the origin, which goes exponentially or faster to zero for large r and which is bounded for all intermediate valuas of r the Schroedinger equation (2.6) can be rewritten as (Calogero 1967) (in a.u.)

$$\frac{d}{dr}\eta_l(E,r) = -\frac{V(r)}{\sqrt{E}} \left\{ \cos\eta_l(E,r) j_l(r\sqrt{E}) - \sin\eta_l(E,r) n_l(r\sqrt{E}) \right\}^2 \qquad (2.22)$$

Apparently V_{MT} satisfies the above conditions and we immediately note that $\eta_l(E,R) = \eta_l(E,\infty) \equiv \eta_l(E)$. This justifies (2.21). So, using (2.21) and (2.19), equations (2.13) and (2.18) give a "phaseshift" description of the bandstructure. In this way the quantities $\alpha_l(E)$ and $\gamma_l(E)$ are transformed into the more familiar $\eta_l(E)$.

We note that the $\eta_l(E)$ arising from (2.20) suffer a "modulo π" ambiguity. Solving (2.22) for the real potential $V_{MT}(r)$ yields:

$$\eta_l^{rp}(E) = n_l\pi + \eta_l(E) \qquad -\frac{\pi}{2} \leq \eta_l(E) < \frac{\pi}{2} \qquad (2.23)$$

where n_l equals the number of bound l-states of $V_{MT}(r)$. In (2.23) is is assumed that $E > 0$ and that E is sufficiently small. (Levinsons theorem). In this sense $\eta_l(E)$ is often called the "reduced phase shift" and apparently only these phase shifts are determining the

bandstructure of the conductionband for energy E (see eq.(2.21) and (2.13). In addition the $\eta_l(E_F)$ are usually small for $E_F \approx E_F^o$ in nearly free electron metals. It is just the possibility of replacing now the strong potential $V_{MT}(r)$ by a weak scattering effective pseudo potential with scattering properties $\eta_l(E)$ which is the fundamental justification of the pseudo potential formalism and which accounts for the great successes of the latter in the past ten or twenty years.

We can introduce a "generalized" Friedel sum

$$Z^{rp}(E_F) = \frac{2}{\pi}\sum(2l+1)\,\eta_l{}^{rp}(E_F) \tag{2.24}$$

Substituting (2.23) into (2.24) leads to

$$Z^{rp}(E_F) = Z^{ion} + Z(E_F) \tag{2.25}$$

with

$$Z^{ion} = 2\sum(2l+1)n_l \tag{2.26}$$

and

$$Z(E_F) = \frac{2}{\pi}\sum(2l+1)\eta_l(E_F) \tag{2.27}$$

From Levinson's theorem for E_F being suitable small we expect for a closed shell ion

$$Z^{ion} = N_A - Z_v \tag{2.28}$$

in which N_A is the atomic number and Z_v is the valence of the metal. Using the semi-empiric $V_{MT}(r)$ for white tin (Devillers et al, 1969) we verified (2.28) by solving (2.21) numerically.

About the value of the Friedelsum $Z(E_F)$ there is little to say off-hand. Originally Friedel's formula is derived for a single positive charge δZ placed in a uniform electron gas with Fermi energy E_F. Then

$$\delta Z = \frac{2}{\pi} \sum_{l} (2l+1)\eta_l(E_F) \qquad (2.29)$$

From this one might expect in the case of a metal the Friedel sum to be

$$Z(E_F) = Z_v \qquad (2.30)$$

suggesting a picture of the metal to be built up from neutral atoms, each carrying its total atomic electron cloud. But as the individual atom potentials overlap in a metal the muffin tin zero will be lower than the zero of the potential of the free atom (Ziman, 1965), so the phase shifts will be measured at a large energy in the former case.

Consistent to first order with (2.30) is (Cohen and Heine, 1972)

$$\lim_{q \to 0} V(q) = -\frac{2}{3} E_F^0 \qquad (2.31)$$

suggesting $E_F = \frac{1}{3} E_F^0$

(2.30) with $Z(\frac{1}{3}E_F^0)$ we will call the "Friedel picture"

II.6 Lloyd picture.

Edwards (1962) has given a treatment of electron states in disordered systems for weak potentials using Green's function theory. Lloyd (1965, 1966) has given an extension of Edwards theory for stronger energy dependent pseudo potentials. For a detailed presentation of their results we refer to those papers. Here we will give briefly some of their results (in a.u.). Lloyd derived an expression for the integrated density of states

$$N(E) = \int_{-\infty}^{E} n(E)\, dE \qquad (2.32)$$

He found

$$N(E) = -\frac{1}{\pi V}\mathrm{Im}\left[\mathrm{Tr}\left\{\ln(k^2 + \Gamma - E - i\varepsilon)\right\}\right] \qquad (2.33)$$

where k^2 and Γ must be understood as the kinetic energy operator and the potential operator respectively.

In momentum representation this results in

$$N(E) = -\frac{1}{\pi V}\mathrm{Im}\left[\ln\left\{\det \| \quad (k^2 - E - i\varepsilon)\,\delta_{\vec{k},\vec{k}'} + \langle\vec{k}|\Gamma|\vec{k}'\rangle \|\right\}\right] \qquad (2.34)$$

Using a t-matrix expansion for Γ Lloyd shows that (2.34) can be rewritten in position representation

$$N(E) = N_0(E) - \frac{1}{\pi V}\mathrm{Im}\left[\ln\left\{\det \| \delta_{L,L'}\,\delta^{\vec{l},\vec{l}'} + t_{(L)}G_{L,L'}(\vec{l}-\vec{l}')\|\right\}\right] \qquad (2.35)$$

with L short for l,m and

$$N_0(E) = E^{3/2}/(6\pi^2) \qquad E>0 \qquad (2.36)$$

$$t_{(L)} = E^{-1/2}\mathrm{tg}\eta_L \qquad (2.37)$$

and

$$G_{L,L'}(\vec{r}) = \begin{cases} -4\pi i E^{1/2}\sum_{L''} c^{L,L',L''} i^{L''} Y_{L''}(\hat{r}) h^{(+)}_{L''}(E^{1/2}r) & |\vec{r}|>R \\ -iE^{1/2}\delta_{L,L'} & |\vec{r}|=0 \end{cases} \qquad (2.38)$$

with $C^{L,L',L''}$ a Clebsch-Gordan coefficient and $h^{(+)}_{L''}$ a Hankel function.

The expression (2.35) is valid for any arrangement of the scattering centers. Now from this point we can proceed for the case of a muffin tin potential taking $E = E_F$ and taking only single center scattering in (2.35). Then because

$$N(E_F) = \frac{4}{3}\pi k_F^3 / (2\pi)^3 = Z_v / 2\Omega_{atom} \qquad (2.39)$$

it follows in a straight forward way that

$$Z_v = Z_v(E_F / E_F^o)^{3/2} + Z(E_F) \qquad (2.40)$$

We will call expression (2.40) the Lloyd picture. Clearly this deviates from the Friedel picture (2.30) for $E_F = \frac{1}{3}E_F^o$. From (2.40) we read off, that $Z(E_F^o) = 0$ and that $dZ(E_F)/dE_F = - Z_v / \frac{2}{3} E_F^o$ for $E_F = E_F^o$, both results which have been derived too by Devillers (1971) from considerations of the KKRZ matrix elements. This should be so, because the Lloyd picture and KKRZ both are basically derived from the same Green's function approach to the nearly free electron states in a metal. Lee (1968) also found the result (2.40) from heuristic arguments.

II.7 Small energy limit of $\eta_l(E_F)$ and of $Z(E_F)$

As experimentally found by Devillers (1971) for very small values of E_F (in practice $E_F < .1\ E_F^o$) the phase shifts obey the rules of general scattering theory i.e.

$$\lim_{E_F \to 0} \eta_l(E_F) = a_l E_F^{(2l + 1)/2} + n_l \pi \qquad (2.41)$$

and this conflicts with the Lloyd picture. Because, by inspection of (2.41) and (2.27), it is clear that $Z(0)$ can only take the values

$$Z(0) = 0, 2, \ldots \qquad (2.42)$$

So for example the Lloyd picture (2.40) would yield $Z(0) = 1$ for the alkalis and the noble metals. In fact it will turn out in the next chapters that always experimentally for Sn, Cu, Ag, Au, Hg the phase shift $\eta_0 \to \pi$ and $\eta_l \to 0$ for $l \geq 1$, so $Z(E_F) \to 2$, when $E_F \to 0$.
None the less the Fermi surfaces of these metals can still be described

well in the APW and KKRZ schemes.

O.K. Andersen (1972) has worked out this idea still further by noting that the structure constants in the KKR formalism can be calculated very easily if E_F is taken to be zero, thus making a band-structure calculation very fast computationally.

II.8 Modified t-matrix

Devillers et al (1973a) have proposed that a "modified t-matrix", rather than the usual t-matrix, be used in Ziman's "weak perturbation" expression for the specific resistivity of a liquid metal (see app. B).

In the near future a formal proof of the above proposal will be given (Devillers, 1974, to be published). The basic idea is, that for a given muffin tin potential and Fermi energy E_F, the s-matrix of a single scatterer is completely determined and is independent of the kinematics of the scattered electrons.

Here we will give only the preliminary results. The modified t-matrix is given by

$$t(E_F, \theta) = \sum_l (2l+1) t_l(E_F) P_l(\cos\theta) \tag{2.43}$$

with

$$t_l(E_F) = -\frac{m^*}{k_F} \exp(i\eta_l) \sin\eta_l \tag{2.44}$$

A modified expression for the optical theorem is

$$\mathrm{Im}\{t_l(E_F)\} = -\frac{k_F}{m^*} |t_l(E_F)|^2 \tag{2.45}$$

and for the relation between s-and t-matrix

$$s_l = 1 - 2i \frac{k_F}{m^*} t_l \tag{2.46}$$

Putting the modified t-matrix (2.43) in the expression for the specific resistivity

$$R \propto \frac{1}{v_F^2} \int (1 - \cos\theta) \, | t(E_F, \theta) |^2 a(\theta) d(\cos\theta) \qquad (2.47)$$

where $a(\theta)$ is the structure factor, and using the well known relation

$$m^* v_F = k_F \qquad (2.48)$$

a correction factor $(m^*)^4$ to the "lowest" order specific resistivity arises. This correction factor was already proposed by Devillers et al (1973a) for calculating the specific resistivity of liquid mercury in terms of the modified t-matrix. There an original overestimation of the specific resistivity by a factor of about 2.5 is found to be completely cancelled, when the value $m^* = .81$ is used (see app.B).

II.9 E_F-ambiguity; first order approach to the band structure problem; conservation of matrix element in first order and its consequences.

Going ahead with the experimental results, we have found that in APW(KKRZ) the Fermi energy E_F is nearly indeterminate by FS data (Devillers 1969, 1971, 1973 (Sn), 1973 (Hg), Coenen 1972, Lee 1968, 1971, Shaw 1972).

If we look at Γ^{APW} in the OFS approximation and restrict ourselves to first order pseudopotential theory in the NFE model (2.20) and (2.12), one immediately sees that on the diagonal

$$k_F^2 - \Gamma^{APW}(q = 0, \alpha_1, E_F) = E_F \tag{2.66}$$

should hold, while off the diagonal (in the degenerate case)

$$\Gamma^{APW}(q_i, \alpha_1, E_F) = c_i \tag{2.67}$$

should hold. Here q_i are reciprocal lattice vectors, $q_i \leq 2k_F$, $i = 1, \ldots M$ and c_i must be constants independent of E_F. Further as an example let us take the case that there are two different values q_i in (2.67). Then if we take three parameters α_1 we have three equations in three unknowns (see Devillers 1972). This makes E_F indeterminable. In the true APW matrix there is of course E_F and k-dependence in (2.66) and (2.67) and moreover second order effects may be important. But the above discussion makes it plausible that in thatcase also E_F is weakly determined.

Assuming (2.66) and (2.67) to be valid one can reach further conclusions about the dependence of α_1 (E_F, R) upon the variables E_F and R, as has been done by Devillers (1972). There it is shown that

(2.66) and (2.67) result in $\alpha_l (E_F,R)$ being linear functions of E_F, as is experimentally generally found.

Further the existence of "focus-points" of O.K. Andersen (1971) are shown to arise from (2.66) and (2.67). A focus point S_l is defined by

$$[\partial \alpha_l(E_F,R)/\partial E_F]_{R=S_l} = 0 \qquad (2.68)$$

and we define $\alpha_l (E_F,S_l) \equiv \alpha_l (S_l)$. Also from Taylor series expansions around S_l it has been proved (Devillers 1972), that

$$\alpha_l(S_l) = \{\alpha_{l0} + \Delta_l l(l+1) + \tfrac{1}{2}\Delta_l^2 \alpha_{l0} l(l+1) \} / \{1 + + \Delta_l(1 + \alpha_{l0}) + \tfrac{1}{2}\Delta_l^2 l(l+1)\} \qquad (2.69)$$

and

$$\alpha_{l1} = \Delta_l(2\pi R_I)^2 [\, 1 + \Delta_l(1 + \alpha_{l0}) + \tfrac{1}{3}\Delta_l^2 \{ l(l+1) + + (1 + \alpha_{l0})^2 \}\,] \qquad (2.70)$$

where

$$\Delta_l \equiv (S_l - R_I) / R_I \qquad (2.71)$$

and we have assumed that

$$\alpha_l (E_F,R_I) = \alpha_{l0} + \alpha_{l1} E_F \qquad (2.72)$$

So for small Δ_l we can write

$$\alpha_l (E_F,R_I) = \alpha_l (S_l) + \Delta_l (2\pi R_I)^2 E_F \qquad (2.73)$$

which equation holds pretty well as a first approximation in most cases we have met. The radii S_l are expected to lie in the neighbourhood of the Wigner-Seitz radius, especially in densily packed metals where the inscribed sphere of the Wigner Seitz cell fills up to 70% of the total volume. This expectation can be made plausible by looking at the

one dimensional case. Then R_I can be choosen R_{WS}, so the interstitial region has zero volume and E_F is completely indeterminable and $S_1 = R_{WS}$. Something of this reflects in the three dimensional case too. In most cases S_1 is close to R_{WS} (Andersen 1971, Devillers 1972, Shaw et al 1972).

As is shown in Devillers (1972) in practice one may use both the linear approximation to $\alpha_1(E_F,R)$ as well as the focus point parameters in limited ranges of E_F. In larger ranges, say for $E_F = 0$ to $E_F = E_F^o$, both approximations fail.

If a metal is more anisotropic, more q_i in (2.67) should be included generally, and thus E_F becomes a less weak parameter. Or to say in terms of the focus point picture : the inscribed sphere fills less of the total volume, the interstitial region is larger and the WS cell can be described worse by a Wigner Seitz sphere.

II.10 Second order approach to the bandstructure problem.

In second order the diagonal eigenvalue equation in NFE theory becomes

$$\langle \psi^{(1)} | \; -\nabla^2 + \Gamma - E_F \; | \psi^{(1)} \rangle = k_F^2 - E_F + \Gamma_0 - \Sigma^{(2)} = 0 \qquad (2.74)$$

with

$$\psi^{(1)} = \frac{1}{\sqrt{\text{Norm}}} \Big[\; | \vec{k}_F \rangle - \sum_{\vec{q}_n}{}' \; \frac{\Gamma_{q_n}}{|\vec{k}_F + \vec{q}_n|^2 - k_F^2} | \vec{k}_F + \vec{q}_n \rangle \Big] \qquad (2.75)$$

and

$$\Sigma^{(2)} = \sum_{\vec{q}_n}{}' \; \frac{|\Gamma_{q_n}|^2}{|\vec{k}_F + \vec{q}_n|^2 - k_F^2} \qquad (2.76)$$

and where Norm stands for $\langle\psi^{(1)} \mid \psi^{(1)}\rangle$ (In the OFS approximation we replace Γ_{q_n} by $\Gamma^{APW}(q_n, \alpha_l, E_F)$.

It is interesting to calculate the kinetic energy in second order as is done in Devillers (1973), for many times in solid state physics one is working with models where the energy dispersion relation is approximated by $E(\vec{k}) = k^2/m^*$

The kinetic energy $E_{kin} = k^2/m^*$ is given by

$$\langle\psi^{(1)} \mid -\nabla^2 \mid \psi^{(1)}\rangle \approx \langle\psi^{(1)} \mid E_F - \Gamma \mid \psi^{(1)}\rangle \approx$$
$$= E_F - \Gamma_0 + 2\Sigma^{(2)} \qquad (2.78)$$

(see Merzbacker, chapter 16, page 370)

From (2.74) and (2.78) it follows

$$E_{kin} = k_F^2 + \Sigma^{(2)} = k_F^2 (1 + \Delta) \qquad (2.79)$$

where we define

$$\Delta = (k_F^2 - E_F + \Gamma_0) / k_F^2 \qquad (2.80)$$

so

$$m^* = (1 + \Delta)^{-1} \qquad (2.81)$$

Consistent expressions for other physical quantities, up to second order, are

$$\nabla_{\vec{k}} E_{\vec{k}} \propto k_F/m^* \qquad (2.82)$$

$$v_F \propto k_F/m^* \qquad (2.83)$$

$$N(E_F) \propto m^* k_F \qquad (2.84)$$

All this leads to rather simple corrections to first order NFE theory, as for example in the NFE expression for the specific resistivity of liquid metals (Devillers 1973).

II.11 Relativistic RAPW scheme; spin orbit coupling.

When the muffin tin potential is so strong that relativistic effects (Darwin term, mass velocity, spin-orbit coupling) become important one has to solve the Dirac equations rather than the Schroedinger equation (see for example Loucks 1965, Loucks 1967). The logarithmic derivative then is replaced by the quantities (Mattheiss 1966).

$$\alpha_l = \left\{ (l+1)R_I \left[cf/g\right]_{-l-1} + lR_I \left[cf/g\right]_l \right\} / (2l+1) \qquad (2.85)$$

$$\beta_l = \left\{ R_I \left[cf/g\right]_{-l-1} - R_I \left[cf/g\right]_l + (2l+1) \right\} / (2l+1) \qquad (2.86)$$

where cf and g are physically allowed solutions of the radial Dirac equations for $E = E_F$. In the non relativistic limit e.q. the light velocity $c \to \infty$, $[cf/g]_{-l-1} \to \alpha_l(E_F,R) - l$ and $[cf/g]_l \to \alpha_l(E_F,R) + l + 1$, so $\alpha_l \to \alpha_l(E_F,R)$ and $\beta_l \to 0$.

As noted by Mattheiss (1966) relativistic effects like the Darwin term and the mass velocity are diagonal with respect to the electron spin and therefore they are included automatically in the α_l's, if these are used as adjustable parameters (see also Devillers 1969).

Mattheiss (1966) has given an explicit expression for the RAPW matrix element (in c.u.)

$$\langle \vec{k}_i, \pm | H-E | \vec{k}_j, \pm \rangle =$$

$$= (\vec{k}_i \cdot \vec{k}_j - E)\delta_{ij} - \frac{4\pi R^3}{\Omega_{atom}} (\vec{k}_i \cdot \vec{k}_j - E) \frac{j_1(2\pi|\vec{k}_i - \vec{k}_j|R)}{2\pi|\vec{k}_i - \vec{k}_j|R} \begin{pmatrix} 1 & 0 \\ 0 & 1 \end{pmatrix} +$$

$$+ \frac{R}{\pi\Omega_{atom}} \sum (2l+1)\alpha_l j_l(2\pi k_i R) j_l(2\pi k_j R) P_l(u) \begin{pmatrix} 1 & 0 \\ 0 & 1 \end{pmatrix} +$$

$$+ \frac{R}{\pi\Omega_{atom}} \sum (2l+1)\beta_l j_l(2\pi k_i R) j_l(2\pi k_j R) P_l'(u) \begin{pmatrix} in_z & n_x + in_y \\ -n_y + in_x & -in_z \end{pmatrix} \qquad (2.87)$$

in which $u = \vec{k}_i \cdot \vec{k}_j / k_i k_j$, $\vec{n} = \vec{k}_i \times \vec{k}_j / k_i k_j$ and P_l' is the derivative of Legendre polynomial P_l.

The last term in (2.87) is purely due to spin orbit coupling. Of course $l=0$ does not contribute, reflected in (2.87) in that $P_o' = 0$. As for the higher values of l the centrifugal term in the radial eigen value equations is dominating the potential term, β_l becomes small. For instance in white tin only the $l=1$ term has a significant influence on the FS (see app.A).

II.12 (R)APW scheme for crystals with more than one atom per primitive cell.

The above theory applies for metals with one atom per primitive lattice cell. If there are more identical atoms per primitive cell this leads in bandstructure theory to the introduction of the well known structure factor S_{ij}

$$S_{ij} = \frac{1}{N_c} \sum_{n=1}^{N_c} \exp(i(\vec{k}_i - \vec{k}_j) \cdot \vec{\tau}_n) \qquad (2.88)$$

$\vec{\tau}_n$ are the positions of the N_c atoms in the primitive cell.

Generally S_{ij} is a complex number, but in those cases where an inversion

point in the primitive cell can be defined, we are allowed to take that inversionpoint as origin, thus making S_{ij} a real number. Most of the more simple crystal structures do have such an inversion point. We can obtain the RAPW matrix elements for these crystals just by multiplying (2.87) with S_{ij}.

$$M^{\pm}_{ij} \rightarrow S_{ij} M_{ij} \tag{2.89}$$

Also if the atoms in the primitive cell are not identical the APW formalism may be extented without much effort. But in this work we do not explore such crystals, the interested reader is referred to the book of Loucks (1967) for the mathematical expressions in that case.

III. COMPUTATIONAL ASPECTS OF APW INTERPOLATION.

III.1 Least squares fit of muffin tin potential parameters to experimental points on the FS in the APW scheme.

The APW energies E for wavevector $\vec{k}$ ($\vec{k}$ in first Brillouin zone) are given by

$$\det \| M(\vec{k}, E, R, \alpha_l(E,R)) \| = 0 \qquad (3.1)$$

where the matrix element is given by (2.12). If we take once and for all $R = R_I$ and we choose $E=E_F$ (because the experimental data are determined at the Fermi energy) then M is only a function of $\vec{k}$ and α_l. Note that the point $\vec{k}$, which satisfies (3.1) is a point on the FS, because $E(\vec{k}) = E_F$ by definition. In practice we choose some line in $\vec{k}$ space along which we are searching for nodes in the determinant. Thus we are finding intersections of that line with the FS. If we know α_l, we can calculate subsequently the points $\vec{k}$ on the FS. But conversely if we know experimentally all points $\vec{k}$ on the FS we can use α_l as adjustable parameters, without knowledge of the muffin tin potential. The question on uniqueness of the α_l so obtained may be deferred to a later stage. From the arguments of section II.2 we assume a small numer of α_l, $l=0,1,\ldots, l_{max}$ to be sufficient, say $l_{max} = 2$. (The α_l with $l_{max}+1 \leq l \leq L_{max}$ are fixed on the "empty potential" values α_l^o).

Further instead of taking all points of the FS, we choose a rather small set of N representative points $\vec{k}_i^{\,exp}$ on the FS, say N = 10. How many of those points should be choosen is a matter of trial and error. Then we have a problem of a $(l_{max} + 1)$ parameter function, which must be fitted to N points. A suitable way to do this is fitting in a least squares sense. Because the determinant is a non linear function of α_l we have to use well chosen values α_l^s as a start for an iterative procedure.

In the least square procedure we are solving the equation

$$(A^T A)(\vec{\Delta\alpha}) = (A^T)(\vec{\Delta\rho}) \tag{3.3}$$

with

$$(\Delta\rho)_i = \rho_i^{exp} - \rho_i(\alpha_l^s) \tag{3.4}$$

$$A_{ij} = (\partial\rho_i(\alpha_l)/\partial\alpha_j)_{\alpha_l^s} \tag{3.5}$$

$$(\Delta\alpha)_j = \alpha_j^n - \alpha_j^s \tag{3.6}$$

where α_j^n is the improved new value of α_j and $\rho_i(\alpha_l^s)$ is the intersection of a line with the FS, corresponding with ρ_i^{exp} on that line. α_l^n can be used as α_l^s in (3.5) and (3.3) in a next iterative step. We iterate the procedure until the root mean square

$$(\Delta\rho)_{rms} \equiv \frac{1}{N} |\vec{\Delta\rho}| \qquad (3.7)$$

has converged to within preset limits. Mostly a few iterations are sufficient.

Accidentally a degeneration of energy levels is not removed by the perturbing potential. Then the determinant has a "parabolic zero", instead of a node, as a function of $\vec{k}$.
We have made our computer programme so that such double nodes are detected as points of the FS too. Those are interesting points because there, in $\vec{k}$ space, magnetic breakdown occurs in de Haas van Alphen experiments.

III.2 Convergence aspects; size of the determinant; Löwdin procedure.

In practice we have to limit ourselves to a finite number of reciprocal vectors as well as to truncate the infinite l-summation at L_{max} (see section II.2). To determine numerical convergence we will use two criteria

1) $(\Delta\rho)_{rms}$ should not change more than some tolerance, say 10^{-4} c.u.
2) The parameters must stay stable against enlarging the number of $\vec{K}$-vectors.

In practice $L_{max} = 6$ suffices and the number of $\vec{K}$-vectors is about 100.
As the numerical evaluation of a determinant of rank M involves a number of multiplications proportional to M^3, working with $M = 100$ would consume an intolerable amount of computer time. Therefore we use a

theory of Price (1950) and Löwdin (1951) which anables us to work with much smaller ranks without loss of accuracy. The trick is to divide the zeroth order eigenvalues $|\vec{k}+\vec{K}_i|^2$ into two groups $|\vec{k}+\vec{K}_i|^2 \leq E_1$ and $E_1 < |\vec{k}+\vec{K}_i|^2 \leq E_2$ and to ignore "interactions" between states of the second group. Then the APW matrix takes the form

$$M^{APW} = \begin{pmatrix} A & A_B \\ A_B^* & B \end{pmatrix} \qquad (3.8)$$

with B a diagonal matrix and always det B $\neq$ 0 for the eigenvalue $E = E_F$ ($E_F < E_1$). Now for calculating det $\| M^{APW} \|$ one first "sweeps" the matrix elements of A_B^*, thus folding in group A_B matrix elements into matrix A, and then solves the determinant of A exactly. The values of E_1 and E_2 are determined by trial and error such that the above criteria are satisfied. Mostly the size of A is about 10 to 20, which leads to the saving of a large amount of computertime.

Another time consuming point in the calculations involves the spherical Bessel functions and Legendre polynomials occuring in the APW matrix elements.

We tabulated these functions in the beginning of the program, mostly at a mesh of .01 in the arguments. We used linear interpolation of the tabulated values.

III.3 Ambiguity in the sign of Fourier transforms in first order perturbation theory.

In first order local pseudo potential theory one is dealing with an ambiguity in the Fourier transforms of the pseudo potential. This can be demonstrated in the simple case of a two fold degenerate zeroth order energy eigen value $E_o = (\vec{k})^2 = |\vec{k} + \vec{K}|^2$. This energy level is split up by the pseudo potential in $E_{\pm} = E_o \pm |V_{\vec{K}}|$ where $V_{\vec{K}}$ is the Fourier transform. So if we know experimentally the energy levels E_+ and E_- we can fit only the absolute value of $V_{\vec{K}}$. In section II.4 we pointed to the similarity between $\Gamma^{APW}(q_n, \alpha_1, E_F)$ and V_{q_n}. If we were fitting Γ^{APW} to first order in the above case we would find <u>two</u> local minima of $(\Delta\rho)_{rms}$ defined on parameterspace, both nearly equally low.

A more complicated example is handled by Devillers et al (1973), (see appendix B) who report an APW fit to the FS of solid mercury. The most important V_{q_n} are V_{100} and V_{110}, leading to <u>four</u> local minima in $(\Delta\rho)_{rms}$. But by taking into account non locality (as is inherent to the APW scheme) and second order effects, and by using accurate FS data an unambigous form factor for mercury was arrived at.

The $\alpha_l(\vec{E}_F,R)$ resulting from rather accurate ab initio muffin tin potentials may help to point to the right solution also.

We note, that the above alternative solutions are approximately symmetrical with respect to the free electron (i.e. $V_{MT} = 0$) case. This may cause trouble in the APW scheme too, because the computer program is "feeling" all alternatives simultanously and it starts to approach one of the local minima on rather spurious "indications".

III.4 Least squares fit in the relativistic APW-scheme.

Making our calculations relativistic aggravates the numerical problems considerably at first sight because

a. each non relativistic matrix element is replaced now by a 2x2 matrix (eq.2.87) thus doubling the size of the determinant, which makes the computation time about 2^3 times longer.

b. all matrix elements become complex numbers now, which makes a factor 4 in multiplications and divisions

c. each node in the constant E search becomes a "parabolic zero"

Fortunately we can eliminate the disadvantages of a and c by making use of the hermitian character of Γ^{RAPW} and of the special features of the spin orbit matrix (Loucks 1967). The hermiticity quite generally assures us that after we have "swept" two rows and columns in the computional procedure of the determinant, the remaining " sub-determinant" matrix is hermitian again.

The 2x2 matrix Γ^{RAPW}_{ij} has the form (2.87)

$$\Gamma^{RAPW}_{ij} = \begin{pmatrix} \Gamma^{++}_{ij} & \Gamma^{+-}_{ij} \\ -(\Gamma^{+-}_{ij})^* & (\Gamma^{++}_{ij})^* \end{pmatrix} \qquad (3.8)$$

so we only have to calculate Γ^{++}_{ij} and Γ^{+-}_{ij} at each step in the "sweep" procedure, thus gaining back the 2^3 factor in computer time. Further we note that all Γ^{+-}_{ii} are zero and this remains so after the sweep procedure has been completed.

So, as the two roots (spin + an -) of the determinant always coincide, we can find those roots by bringing Γ^{RAPW} into the triangular form Γ^D and then taking the product $\prod_i \mathrm{Re}\Gamma^D_{ii}$ instead of $\prod_i (\Gamma^D_{ii})^* \Gamma^D_{ii}$.

III.5 Least squares fit to dHvA data.

Quite analogously to section III.1 one can determine the APW parameters by fitting on de Haas van Alphen (dHvA) extremal cross sectional areas instead of on calipers. Then we have to replace ρ by S in equations (3.3), (3.4) and (3.5). Of course area fitting consumes considerably more computertime than caliper fitting.

IV. RESULTS

IV.1 White tin.

As a severe test for the muffin tin model we judged the FS of white tin to be a good test case. Its FS was well established experimentally by the work of Stafleu et al (1967), Craven et al (1968) and Matthey et al (1971, 1973).

Especially the RF size effect measurements of Matthey were very inviting, for several reasons. First they had the obvious advantage of delivering a lot of $\vec{k}$ points on the FS, which saves computertime by orders of magnitude compared with dHvA fitting. Second they were claimed to be very accurate. Third that part of the RFSE measurements which could hardly be interpreted directly, for example because they were arising from non central orbits, from cut-offs in $\vec{k}$ space or from breaks, hopefully could be assigned in the RAPW calculated projections of the FS.

The results of our calculations have been reported in Devillers et al (1969, 1973). The latter paper has been included in this thesis as appendix A. The reader is asked to study this appendix at this point.

Here we only will make some general remarks.

The selection of the $\vec{k}$ points on which we will fit the logartihmic derivatives is based on several criteria:

a. the interpretation of the experiment should be as unambiguous as possible

b. the experimental error should be small; on the 14 selected points the mean absolute error is .0 03 c.u.

c. The points should be spread over the FS more or less uniformly. This provides maximum assurance that there are enough independent equations in the least squares procedure to enable a stable fit to be made.

d. enough points should be selected, which are as much as possible sensitive to the crystal potential, i.e. points which are degenerate in the FE model and are split up by the crystal potential.

On the basis of the above points we have selected 14 points on the FS. From table 2 of app. A we see that with as few as four α_1 we easily can fit to within the experimental error. The discussion of the apparent E_F ambiguity is postponed to the next chapter.

To check further how RAPW works as an interpolation scheme we have calculated another selected group of about 60 $\vec{k}$-points (or better its projection) spread over the whole FS and compared them with the experimental values (table 4 of app.A). The agreement is excellent : mean absolute deviation .002 c.u. and a largest absolute deviation .010 c.u. The latter result in turn confirms our initial selection of 14 points to be sufficient.

Further the projection of the FS to three symmetry planes (100), (110) and (001) have been calculated (section 3 and figures 3-11 of app. A). Nearly all the RFSE measurements of Matthey et al (1971) could be placed in those projection figures, where the work of Matthey (thesis, 1969) and of Matthey et al (1973) of course was extremely helpful for the interpretation.

All details are found in section 3 and figures 3-11 of app.A. At this point we only wish to draw the attention to a few of the details to illustrate the high quality of the RAPW interpolation scheme :

a. the curve 9'10 in fig.7 is the projection of the fourth zone "neck" on (001); this opening does not exist in the free electron model. Thus this opening is very sensitive to the crystal potential. We note a splendid agreement between the RAPW calculated curve and the RFSE resonance c21 (see also table 4).

b. a piece of the FS, which does not exist in the free electron zone, is the sixth zone around W. As the projection on (100)(fig 11a) and on (110) (fig 11b)have no inversion centre one has to interpret the RFSE measurements via a "tangential construction" (see section 3 of app. A). Doing so we note an agreement to within a few thousands of k_o between the RAPW curves and the experimental calipers. Further fig.11a shows the existence of <u>two</u> extremal cross sections, differing by a few per cent (table 5 of app.A). This is nicely confirmed experimentally (footnote <u>e</u> at table 5).

c. special cut off points like 7' in fig. 8 and 13' in fig. 9 may arise, when two projection curves merge, and give rise to the resonances a37, a38 and b6. 7' and 13' again are very "potential sensitive" and although they are not fitted directly, the RAPW values agree to within .001 k_o with experiment (see table 4 of app.A).

d. as an example of non central orbits, which are not interpretable without the calculated projection curves we mention b13 in fig.9. The experiments confirm exactly our calculations (see also table 4 of app.A)

We have to compare also with other available information on the geometry of the FS like dHvA data (table 5 of app.A). The agreement is not quite satisfying, because the main relative deviation of 1.5% with especially the measurements of Craven et al (1968), who claims an experimental error of 1%, is slightly outside this experimental error. In the discussion of section 4 of app.A some possible sources of the discrepancies are suggested.

In conclusion we may say that the RAPW scheme indeed is very well suited for interpolation of the FS data on white tin.

IV2. The noble metals.

As a second test for FS parametrization with muffin tin parameters we have choosen the noble metals (Coenen et al 1972). For two reasons they are interesting in this respect.

a. The FS consist of one multiple connected single zone. dHvA data of a very high precision are available, such that FS radii have been determined to within a few times 10^{-4} c.u.

b. for the noble metals it is well established that there is a narrow d-band in the s conduction band. This makes a local pseudo potential fit inadequate whereas APW,KKR,KKRZ give full attention in a natural way to the l-dependence of the pseudo potential.

From the work on FS parametrization we mention : Lee (1969), who performed an APW analysis for Cu; Coenen et al (1972), who made a KKRZ interpolation and Shaw et al (1972) who used KKR. In general their findings agree very closely. For the sake of clearness we will restrict ourselves to a discussion of the work of Coenen only.

The first remark is that although the FS is known better than that of white tin by almost a factor of ten the quality of the fit is again to within experimental inaccuracy.

Second the parameter E_F is even less well determined than in the case of white tin ; Coenen has investigated the quality of fit for the range .01 c.u. $< E_F <$. 80 c.u. (E_F^o= . 61 c.u.) and he has not found serious loss of quality.

Third, mostly the influence of the non constant part of the crystal potential in the interstitial region is judged to be negligible. But keeping in mind the accuracy with which the FS has been describes (order 10^{-4} c.u.) Coenen thought it useful to investigate this numerically. To obtain some reasonable values for ΔV_{111} and ΔV_{200} he Fourier analys ed a smoothly extrapolated ab initio muffin tin potential of Christensen (1969). The ΔV_{ij} obtained can be included in the KKRZ (or APW) formalism easily by the analysis of Beleznay and Lawrence (1968). Coenen found the ΔV_{ij} so computed to be of negligible importance as to the quality of fit and as to the Friedelsum, but not as to the phase shifts. These latter phenomena can be understood from our analysis of the E_F ambiguity. Eq. (2.66) and (2.67) now read

$$k_F^2 - \Gamma^{KKRZ}(q=0,\ \bar{\eta}_l, E_F) = E_F \qquad (4.1)$$

$$\Gamma^{KKRZ}(q_i,\ \bar{\eta}_l, E_F) + \Delta V(q_i) = c_i \quad i=1,2 \qquad (4.2)$$

so we have three new equations in the new phase shifts $\bar{\eta}_l$ and this is equally well solved, albeit that $\Delta V(q_i) \neq 0$ will yield $\bar{\eta}_l$ instead of η_l. As the diagonal eq. (4.1.) is unaltered and as

$$\Gamma^{KKKRZ}(q=0,\ \eta_l, E_F) \approx -\frac{2}{3}E_F^o\ Z(E_F)/\ Z_v \text{ for } E_F \approx E_F^o$$

(see Devillers, 1971) eq.(4.1) tells us that the Friedel sum will not be influenced by including $\Delta V(q_i)$. This remains nearly true also if we were to replace (4.1) by the second order diagonal equation (compare with (2.74)).

IV.3 Mercury.

The place of solid and liquid mercury in band structure theory is a very peculiar one. In the last ten years a steady stream of publications has appeared reflecting many efforts to resolve the extravagant physical properties of mercury.

First of course there is the problem that it is a liquid metal at room temperature. This raises a lot of difficulties in preparing single crystals to do dHvA and other Fermi surface investigations, and thus this is the reason, why experimentalists only the last six

years have done extensive experiments on it. We mention dHvA experiments of Brandt and Rayne (1966), magneto resistance measurements of Dishman and Rayne (1968), magneto accoustic measurements of Bogle, Coon and Grenier (1969). These authors also performed local pseudo potential fits, resulting in $V(q_n)$, which were in poor quantitative agreement with each other; as they were also in poor agreement with ab initio model potential calculations of Animalu and Heine (1965). But the results agreed with each other in that the FS of Hg is free electron like. The free electron model consist of a multiply connected first zone hole piece, "centered" around (111) and (110) BZ faces and a second zone electron lens, centered in L. As the free electron spheres touches the (111) and (110) BZ faces very nearly, the pseudo potential easily produces openings around T and X (see fig. 1 of app.B for the location of these symmetry points in the BZ).

Second, despite the experimental evidence for a nearly free electron like FS, the above mentioned pseudo potential form factors yielded large discrepancies between the experimental value of the specific resistivity of liquid mercury at room temperature and the values, calculated with Ziman's weak perturbation expression for this quantity

$$R_s \propto \int_0^{2k_F} a(q) \, |V(q)|^2 q^3 dq \qquad (4.3.)$$

where a(q) is the structure factor, i.e. the Fourier transform of the pair distribution function of the scattering centers. Experimentally a(q) may be determined accurately from neutron scattering or X-ray scattering experiments. As the integrand contains a factor q^3 and as a(q) is peaked near $q = 2k_F$, the value of Rs is strongly dominated by the value of V(q) for $.6 < q/2k_F \leq 1$. This is the region, where also the lowest q_n for solid mercury are lying. All the above pseudo potentials yielded an underestimation of the anomalously high value $R_s^{exp} = 96\ \mu\Omega\,cm$, for example by a factor of three for the Animalu-Heine - modelpotential. This has been worrying a lot of people for years.

Third, experimentally the specific resistivity of the liquid metal drops fast when it is alloyed with many other metals. This is an anomalous phenomenon compared with most other metals, where the specific resistivity grows under alloying usually. The latter is made plausible by reasoning that the disorder of the medium is augmented by the foreign guest atoms. Mott (see his recent review article, 1972) tried to explain this anomaly of mercury by assuming a pseudo gap in the density of states of liquid mercury. This pseudo gap arises in his theory, when the mean free path of the conduction electrons becomes about the mean atom distance. A pseudo gap of about $[N(E_F) / N(E_F^o)]^2 = .5$ would explain the anomalous resistivity drop, assuming that the pseudo gap fills up quickly on alloying. Later on he with drew this explanation, because of Edwards cancellation theorem (Edwards 1962), which states that every $N(E_F)/N(E_F^o) \neq 1$ cancels in the expression for R_s.

Fourth, experimentally the Hall coefficient is very nearly free electron like ($R_H=(nec)^{-1}$)

Fifth, another physical quantity, the volume derivative of the specific resistivity at the melting point is anomalously high experimentally.

Sixth, from the RAPW calculation of Keeton and Loucks a 5d - band appeared, lying <u>in</u> the conduction band.

To explain the above experimental points a peculiar form factor was suggested by Evans, Greenwood, Lloyd and Ziman (1969) and Evans (1970) (see fig. 2 of app.B). Indeed the above points two and three can be explained with it. But not the fifth and sixth point (see app.B). For as to the latter point it may be argued from scattering theory, that the d-band is a "resonant state" band. This means that the l=2 shift behaves like

$$\mathrm{tg}\eta_2 = \frac{\Delta_2}{E_{res} - E} \qquad (4.4)$$

(see fig.1)

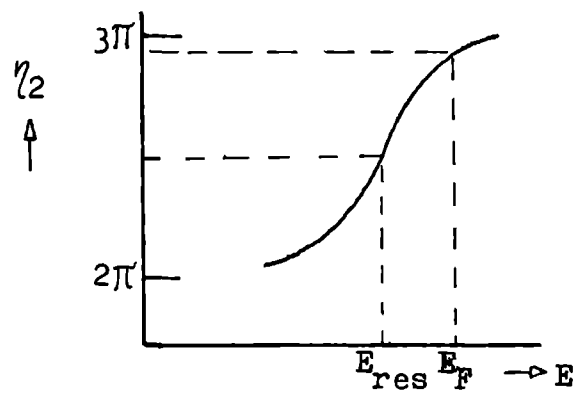

Fig.1 η_2 as a function of energy for a resonant state band

So $\eta_2(E_F)$ is expected to be rather large negative, where as η_1 of Evans is rather large positive ($\sim$.2rad). Moreover this positive value of η_2 conflicts with the results of phase shifts fitting of Lee (1969), Coenen et al (1972) and Shaw et al (1972) on the FS of the noble metals, where it was always found η_2 to be negative which in turn is consistent with a large number of ab initio band structure calculations on those metals, where a d-band resonance in the s-p band was found.

The latter considerations especially motivated us to use our APW interpolation scheme for the accurate dHvA measurements of Poulsen et al (1971) in order to investigate which set of phase shifts would be most consistent with FS data. (we are grateful to Prof. W.H. Young, who initially drew our attention to the "mercury problem"). The results have been reported by Devillers et al (1973a) and by Devillers et al (1973b), these papers being included as appendices B and C respectively. App.B reports the investigation of the various local minima in the rms deviation in dHvA fitting. In particularly it turns out that the Evans version of the form factor is unlikely mainly because it does not yield any"β-arms" in the X BZ-face, a point which was also mentioned by Jones and Datars (1971). By the arguments listed in app.B it turns out that the previous Animalu-Heine shape is the correct one, albeit that our form factor is much stronger in the backward scattering region. This results now in an <u>overestimation</u> of the experimental value of the specific resistivity (compare with the above point two). This problem

has been resolved too in app.B, where we introduce a second order correction factor m^*. We derived an expression for this quantity by adopting ideas of Edwards (1962). There a complicated expression for $\Sigma^{(2)}$ in the liquid is given, the calculation of which needs the evaluation of the principal part of an integral with a singularity in its integrand. In our case we can circumvent this numerical problem by eliminating $\Sigma^{(2)}$ via eq.2-8 of app.B, which are taken as the analogy of eq. (2.74) - (2.81). As is discussed in app.C due to our fit procedure Γ^{APW} is accurate to all orders, so assuming third and higher orders may be neglected, $\Sigma^{(2)}$ is exactly given by eq.(2.74). At given k_F^2 and E_F, Γ_o is easily evaluated via eq (2.20). From table 2 of app.B we note that, for $E_F \approx \frac{1}{3} E_F^o$, $m^* = .81$. From eq. (2.84) it follows then $N(E_F)/N(E_F^o) = .81$, or a pseudo gap in the density of states in the sense of Mott (see discussion point three of this section). Very recently Cotti et al (1973) have found experimental evidence for such a pseudo gap from photo emmission experiments. From their figures we estimate $N(E_F)/N(E_F^o) \approx .8$ for both solid and liquid mercury, which result provides another strong support for our form factor.

As to the interpolated Fermi surface we note some asymmetries, which have not been recognized earlier (fig.2 of app.C). Indeed there is some experimental evidence for these asymmetries (see app.C)

In conclusion we may say, that the results on mercury form a third example of how very well the muffin tin model works for metals and of what kind of useful applications of the obtained parameters there are.

IV. 4 Experimental behaviour of α_1, η_1 and Z as a function of E_F.

In all former cases (Sn, Cu, Ag, Au, Hg) the logarithmic derivatives show nearly linear behaviour as discussed in section II.9, even in the low E_F region.
Also in all cases the low E_F behaviour of the phase shifts is similar to the low energy behaviour eq.(2.41) for a constant potential. However the limit $\eta_1(E_F) \to 0$ mod.π does not mean $\lim \alpha_1(E) = \alpha_1^o$ (E=0) as will be shown. The limit value

$$\alpha_1(0,R) = \lim_{E_F \to 0} \alpha_1(E_F,R) \tag{4.5}$$

can be computed if the coefficients in (2.41) are known.
For example in white tin the "scattering lenght" $a_o = .300 \pm .00\ 3$ c.u. (Devillers et al 1971).
Then, with R = .259 c.u., we obtain easily via a Taylor series expansion of j_1, n_1, j_1', n_1' and $tg\,\eta_1$ in (2.21)

$$\alpha_0(0,R) \approx \frac{a_o}{R - a_o} = -7.3 \pm .5 \tag{4.6}$$

which must be in agreement with the graphically extrapolated value (Devillers et al, 1971) $\alpha_o\ (0,R) = -6.0 \pm 1$.

Eq. (4.6) also exemplifies a weak point of the muffin tin model, i.e. if R is choosen too close to a_o then $\alpha_o \to \pm\ oo$, reflecting a node in the l = 0 wave function for $R = a_o$.
This makes the APW (KKRZ) no longer manageable numerically.

One should always choose R such that one is avoiding that kind of accidental singularity , or one should choose a slightly modified APW scheme. Concerning the Friedelsum for the above metals we always found $Z\,(E_F^o) \approx 0$ and $Z\,(\frac{1}{3} E_F^o) \approx Z_v$. This seems to be in agreement with the Friedel picture (see section II.5). But we can also compare with the Lloyd picture (section II.6). In fig. 2 we have plotted $Z(E_F) / Z_v$ as a function of $(E_F/E_F^o)^{3/2}$. And from the near linear behaviour of $Z(E_F)/Z_v$ in a large region of the argument, it is suggested that the Lloyd picture is the more correct one. The low E_F behaviour is of course dictated by the small energy behaviour of η_1.

As to the linear parts of the Friedel sum versus E_F in fig.2 it seems to be possible to improve upon the Lloyd picture in a simple way by taking into account the effect of orthogonalization on the core states. This leads to a "depletion hole" of charge $d_h Z_v$ (see for example Cohen and Heine 1970). Then the electron density in the interstitial region (and fictively in the whole volume) corresponds to $(1+d_h)Z_v$ valence electrons/atom. So in our opinion an improvement upon the Lloyd picture is

$$Z(E_F)/ Z_v = (1 + d_h)\left[1 - (E_F/E_F^o)^{3/2}\right] \qquad (4.7)$$

From fig.2 we estimate for $E_F > \frac{1}{3} E_F^o$: $d_h = .11 \pm .02$ for white tin and $d_h = .20 \pm .05$ Hg, which values are in agreement

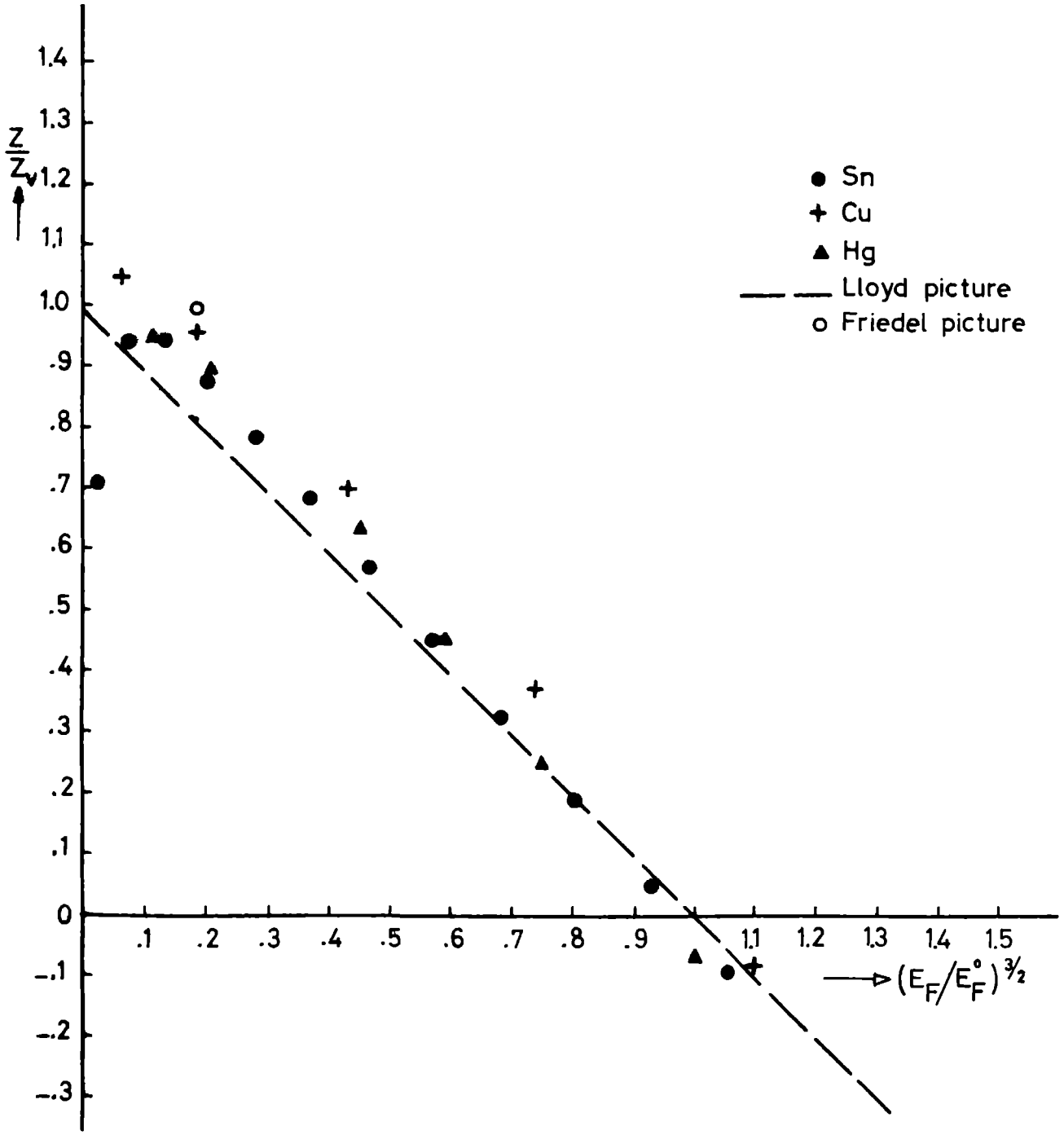

Fig.2. Experimental behaviour of the Friedel sum as a function of $(E_F/E_F^o)^{3/2}$ for white tin, copper and mercury. The data have been taken from Devillers et al (1972) for white tin, from Coenen et al (1972) for copper and from Devillers et al (1973a) for mercury respectively.

with model potential calculated values of Cohen and Heine (1970) : $d_h = .08 \pm .01$ for white tin and $d_h = .26 \pm .02$ for Hg respectively. To give a more accurate description of the experimental Friedel sum there is need for further theoretical refinements. Also it would be interesting to investigate more metals in the above way.

V. SOME APPLICATIONS OF EXPERIMENTAL FS DETERMINED MUFFIN TIN PARAMETERS.

If the experimental muffin tin parameters were to have physical significance, other than that they can be used for an accurate description of FS data, ideally they should be able to describe too other physical phenemona, like the electron-phonon interaction (Lee, 1972; Allen, 1972), bandstructure and FS of compounds, compressibility of the metal and specific resistivity of the liquid metal.
We have met a very interesting test case : the specific resistivity of liquid mercury (section IV.3 and app.B). That the resulting specific resistivity agrees to within a few per cent with the experimental one provides at the same time very strong evidence for the following statements

a. The OFS approximation (2.19) is a very accurate one to the atomic form factor of mercury : in the backward scattering region, because this determines almost completely the specific resistivity (eq.4.3) and also in the forward scattering region, for the second order correction factor m^* ((2.80) and (2.81)) depends totally on $\Gamma^{APW}(0,E_F)$. For example, an error of 0.1 c.u. in $\Gamma^{APW}(0,E_F)$ means an error of 10% in the m^* corrected value of the specific resistivity.

b. the nearly free electron expression for the specific resistivity of liquid metals apparently holds too for cases, where second order effects are significant provided the latter are accounted for by a simple multiplication factor.

c. the anomalously high value of the specific resistivity of liquid mercury is mainly caused by the rather strong d character of the form factor.

Another physical quantity which can be calculated from the atomic form factor is the volume derivative of the specific resistivity. This has been done for the case of liquid mercury (app.B), which has an anomalously high value for that quantity. Because m^* drops out, the good agreement with the experimental value may be especially convincing those who might have looked upon our $(m^*)^4$ correction to the specific resistivity with some scepticism.
A further application of the muffin tin parameters is that they can be used to test ab initio calculated crystal potentials : instead of calculating the FS and of subsequent comparing with experimental data it now suffices to compare the ab initio calculated logarithmic derivatives or phase shifts with the fitted ones, as for example Ament et al (1973) has done recently for the case of white tin, and as Meyer et al (1973) has done for white tin, the noble metals, mercury and the alkali metals.

VI. CONCLUSIONS AND SUGGESTIONS FOR FURTHER RESEARCH.

In this work we hope we have been able to demonstrate that the muffin tin parameters are extremely useful in interpolating geometrical Fermi surface data. We have exemplified this for the metals white tin, the noble metals and mercury. In every case the quality of fit is to within experimental accuracy. Especially for the noble metal this means that the quality of fit is to within a few times 10^{-4} c.u. An apparantly strong E_F ambiguity is quite well understood now.
An analysis from a different view is given by Heine et al 1971.
It is also shown that the APW interpolation scheme can resolve a lot of fine details of the Fermi surfaces and that it is a powerful instrument to facilitate the interpretation of dHvA, RFSE, magneto accoustic, cyclotron resonance and other Fermi surface related physical properties.
It is also shown that the OPS approximation is a very reliable one. The relation between the APW scheme and the more familiar local pseudo potential theory is much clarified. Also the relations between Block theory of crystalline metals and scattering theory of (disordered) densily packed scattering potentials have been clarified considerably. Further it has been shown that the parameters obtained can be used very successfully in the computation of physical properties like specific resistivity (and its volume derivative) of liquid metals.
Suggestions for further research, arising from the work, may be listed in the following way

a. more precise dHvA and / or RFSE measurements to test a lot of RAPW predictions on white tin,

b. the same as in a as to the predicted asymmetries in the Fermi surface of mercury,

c. a more theoretical foundation of our $(m^*)^4$ correction to the specific resistivity of liquid metals in Ziman's weak perturbation theory,

d. testing the APW scheme on the Fermi surfaces of metal compounds might give indications on charge transfer,

e. a theoretical improvement upon the Lloyd picture up to second order.

References

Allen P.B., and Lee M.J.G., 1972, Phys.Rev.B 5, 3848.

Ament M.A.E.A., 1974, to be published.

Andersen O.K., 1971, Phys.Rev.Letters 27, 1211.

Andersen O.K., 1972, private communication.

Animalu A.O.E. and Heine V., 1965, Phil.Mag.12, 1249.

Beleznay F., and Lawrence M.J., 1968, J.Phys.C.(Proc.Phys.Soc.) 1, 135.

Bogle T.E., Coon J.B., and Grenier C.G., 1969, Phys.Rev.177, 1122.

Brandt G.B., and Rayne J.A., 1966, Phys.Rev. 148, 644.

Calogero, F., 1967, Variable Phase Approach to Potential Scattering (New York, Academic Press).

Christensen N.E., 1969, Phys.Stat.Sol., 31, 635.

Coenen N.J., and de Vroomen A.R., 1972, J.Phys.F 2, 487.

Cohen M.L. and Heine V., 1970, Solid State Physics, ed.F.Seitz et al, (Academic Press, New York), vol 24.

Cotti P, Güntherodt H.J., Oelhafen P., Wullschleger J., 1973, Sol.State Comm. 12, 635.

Craven J.E., and Stark R.W., 1968, Phys.Rev. 168, 849.

Devillers M.A.C., and de Vroomen A.R., 1969, Phys.Lett. 30, 159.

Devillers M.A.C., and de Vroomen A.R., 1971, Sol.State Comm. 9, 1939.

Devillers M.A.C., and de Vroomen A.R., 1971, Phys.Rev.B 4, 4631.

Devillers M.A.C., 1972, Sol.State Comm. 11, 395 and erratum.

Devillers M.A.C., Matthey M.M.M.P., and de Vroomen A.R., 1973, to be published in Phys.Stat.Sol.

Devillers M.A.C., Young W.H., and de Vroomen A.R., 1973a, J.Phys.F, Metal Phys. 3, L220.

Devillers M.A.C. and de Vroomen A.R., 1973b, to be published in J.Phys.F, Metal Physics.

Dimmock, 1972, Solid State Physics, ed F.Seitz, (Academic Press, New York), vol.26.

Edwards S.F., 1962, Proc.R.Soc.A, 267, 518.

Evans R., Greenwood D.A., Lloyd P., and Ziman J.M., 1969, Phys.Lett., 30A, 313.

Evans R., 1970, J.Phys.C : Metal Phys.Suppl., 2, S 137.

Heine V, and Lee M.J.G., 1971, Phys.Letters 27, 811.

Johnson K.H., 1966, Phys.Rev. 150, 429.

Korringa J., 1947, Physica XIII, 392.

Kohn W, and Rostoker N., 1954, Phys.Rev.94, 1111.

Lee M.J.G., 1969, Phys.Rev. 178, 953.

Lee M.J.G., 1969, Phys.Rev. 187, 901.

Lee M.J.G., and Heine V., 1972, Phys.Rev.B 5, 3839.

Lloyd P., 1965, Proc.Phys.Soc. 86, 825.

Leigh R.S., 1956, Proc.Phys.Soc, A69, 388.

Loucks T.L., 1965, Phys.Rev. 139, A 1333.

Loucks T.L., 1967, Augmented Plane Wave Method (W.A. Benjamin, Inc., New York)

Löwdin P.O., 1951, J.Chem.Phys., 19, 1396.

Mattheiss L.F., 1966, Phys.Rev. 151, 450.

Matthey M.M.M.P., 1969, thesis Nijmegen.

Matthey M.M.M.P., and de Vroomen A.R., 1971, Sol.St.Comm. 9, 1329.

Matthey M.M.M.P., Devillers M.A.C., and de Vroomen A.R., 1974, to be published in Phys.Stat.Sol.

Meyer A., Young W.H., and Devillers M.A.C., 1973, J.Phys.F.

Mott N.F., 1972, Phil.Mag. 26, 505.

Poulsen R.G., and Datars W.R., 1971, Phys.Rev.B 4, 4202.

Pryce M.H.L., 1950, Proc.Phys.Soc., 63, 25.

Segall B., and Ham F.S., 1968, Methods Comp.Phys. 8, 251.

Shaw J.C., Ketterson J.B., and Windmiller L.R., 1972, Phys.Rev.B 5, 3894.

Slater J.C., 1937, Phys.Rev. 51, 846.

Stafleu M.D. and de Vroomen A.R., 1967, Phys.Stat.Sol. 23, 675.

Ziman J.M., 1965, Proc.Phys.Soc. 86, 337.

Ziman J.M., 1966, The properties of liquid metals, ed. Adams P.D., et al, (Taylor and Francis, London), 551.

Ziman J.M., 1972, Solid State Physics, ed F.Seitz et al, (Academic Press), vol. 26.

LIST OF ABBREVIATIONS

L.C.A.O.	Linear combination of atomic orbitals
KKR	band structure scheme, developed by Korringa, and by Kohn and Rostoker
KKRZ	KKR brought in $\bar{k}$-representation by Ziman
APW	augmented plane wave
RAPW	relativistic augmented plane wave method
OPW	orthogonalised plane wave
OFS	on Fermi sphere approximation
E_F	Fermi energy with respect to muffin tin zero
E_F^o	Fermi energy for free electron gas
FS	Fermi surface
a.u.	atomic units
c.u.	crystal units
NFE	nearly free electron
R_I	radius of inscribed sphere
R_{WS}	radius of Wigner-Seitz sphere
RFSE	radio frequency size effect
dHvA	de Haas-van Alphen effect

APPENDIX A .

The Fermi surface of white tin from a RAPW interpolation.

(reprinted from Physica Status Solidi B, 1974)

THE FERMI SURFACE OF WHITE TIN FROM A RAPW INTERPOLATION COMPARED WITH EXPERIMENT

M.A.C. Devillers, M.M.M.P. Matthey and A.R. de Vroomen

Fysisch Laboratorium, Katholieke Universiteit, Nijmegen, The Netherlands

ABSTRACT

From extensive calculations we will show, that the relativistic APW method, used as an interpolation scheme, can describe the Fermi surface of white tin consistent in detail with all available experimental data. At the same time we will use this model of the Fermi surface of white tin to confirm and to complete the interpretation of radio frequency size effect measurements as presented in the preceeding paper.

Durch ausführliche Rechnungen zeigen wir, dass die relativistische APW Methode als Interpolationsschema die Fermi fläche von Weissem Zinn beschreiben kann, und zwar auf eine bis ins Detail mit den vorhandenen experimentellen Daten konsistente Weise. Zugleich werden wir dieses Modell der Fermi fläche gebrauchen, um die Interpretation der RFSE Messungen zu bestätigen und zu vervollständigen wie das im vorhergehenden Artikel geschehen ist.

1. Introduction.

The purpose of this paper is to investigate the usefulness of the relativistic APW scheme as an interpolation scheme for geometrical data on the Fermi surface (FS) of a polyvalent metal as well as to help complete the global interpretation of the radio frequency size effect (RFSE) measurements on white tin of Matthey et al [1]. In a previous letter [2] we already introduced the method and we presented the preliminary results of our calculations. In this paper we will discuss the method in more detail and we will present an extensive comparison of the calculations with RFSE and de Haas-van Alphen (dHvA) data [3,4,5] as well as with the results of previous plane wave calculations [4,6]. It turns out that the APW scheme is most suitable for interpolation purposes; the few remaining discrepancies between calculation and experimental data are felt to be due more to experimental errors rather than to inadequacies of the APW scheme.

The starting point for our calculations is the APW determinantal equation for the - one electron - energy eigen values of electrons in a perfect metallic crystal. The relativistic APW matrix elements (RAPW) have the form [7,8]:

$$< \vec{k}_i, \pm | H-E | \vec{k}_j, \pm > =$$

$$(\vec{k}_i.\vec{k}_j - E)\delta_{ij} - \frac{4\pi R^3}{\Omega_{at}} (\vec{k}_i.\vec{k}_j - E) \frac{j_1(2\pi|\vec{k}_i - \vec{k}_j|R)}{2\pi|\vec{k}_i - \vec{k}_j|R} S_{ij} \begin{pmatrix} 1 & 0 \\ 0 & 1 \end{pmatrix} +$$

$$+ \frac{R}{\pi\Omega_{at}} \sum_{l} (2l+1)\alpha_l j_l(2\pi k_i R) j_l(2\pi k_j R) P_l(u) \; S_{ij} \begin{pmatrix} 1 & 0 \\ 0 & 1 \end{pmatrix} +$$

$$+ \frac{R}{\pi\Omega_{at}} \sum_{l} \beta_l j_l(2\pi k_i R) j_l(2\pi k_j R) P_l'(u) \; S_{ij} \begin{pmatrix} in_z & n_y+in_x \\ -n_y+in_x & -in_z \end{pmatrix} \qquad (1)$$

in which $u = \vec{k}_i.\vec{k}_j / k_i k_j$, $\vec{n} = \vec{k}_i \times \vec{k}_j / k_i k_j$,

S_{ij} is the structure factor and

$\vec{k}_i$, E, Ω_{at}, R, j_l, P_l, P_l' have their usual meaning.

The information of the muffin tin potential is contained in the dimensionless α_l and β_l, which are constants for a Fermi surface

$$\alpha_l = \left[(l+1)R \{ cf/g \}_{-l-1} + lR \{ cf/g \}_l \right] / (2l+1) \qquad (2)$$

$$\beta_l = R \{ cf/g \}_{-l-1} - R \{ cf/g \}_l + (2l+1) \qquad (3)$$

where cf and g are physically allowed solutions of the radial Dirac equations taken for r = R, R being the muffin tin radius, and the energy $E = E_F$, the Fermi energy relative to the muffin tin zero. In the non-relativistic case $\beta_l \rightarrow 0$ and $\alpha_l = Ru_l'/u_l$, where $u_l'(R,E_F)/u_l(R,E_F)$ is the logarithmic derivative of the l-dependent solution to the Schrödinger equation, evaluated for r = R and $E = E_F$. A non-zero β_l is caused solely by spin-orbit coupling. We note that some relativistic effects like the Darwin term and the mass-velocity term, which may have larger effects on the FS than spin-orbit coupling [8], are diagonal with respect to the electron spin and are therefore included automatically in the α_l's, if these are used as adjustable parameters.

It is instructive to calculate the - reduced - scattering phase shifts $\eta_l(E_F)$ of the muffin tin potential and the Friedel sum $Z_F(E_F)$ from $\alpha_l(E_F,R)$ using the well-known relations

$$tg\,\eta_l(E_F) = \{ xj_l'(x)-\alpha_l(E_F,R)j_l(x) \} / \{ xn_l'(x)-\alpha_l(E_F,R)n_l(x) \} \quad (4)$$

and

$$Z_F(E_F) = \frac{2}{\pi} \sum_l (2l+1)\eta_l(E_F) \quad (5)$$

with $x = 2\pi R E_F^{\frac{1}{2}}$. To give $\eta_l(E_F)$ its usual physical meaning it is assumed that the relativistic effects in $\alpha_l(E_F,R)$ are not too large.

Throughout this paper we will use as units the "crystal units" (c.u.) as introduced in [9,10]. Taking for the crystallographic constant a = 5.812 Å and a/c = 1.841 at 4°K [11] the conversion factor for energy to R_y is .3284 R_y per c.u.; the length ΓL is the unit in reciprocal space.

2. Calculation.

The parameters α_l (short for $\alpha_l(E_F,R)$), l = 0,1,2 and 3, are calculated with the use of a constant E search by fitting them to fourteen selected points of the FS (Fig. 1, Table 1). These points are experimentally well determined by RFSE measurements as reported in the preceeding paper [1]. As the relationship between the co-ordinates of the points on the FS and the α_l is a non-linear one the fit requires an iteration procedure. To start the iteration one may use for the values of α_l and E_F the "empty potential" values or some "rough" values from ab initio bandstructure calculations or preferably those determined from experimental or theoretical values of local form factors of the pseudo potential. The "empty potential" values are taken for

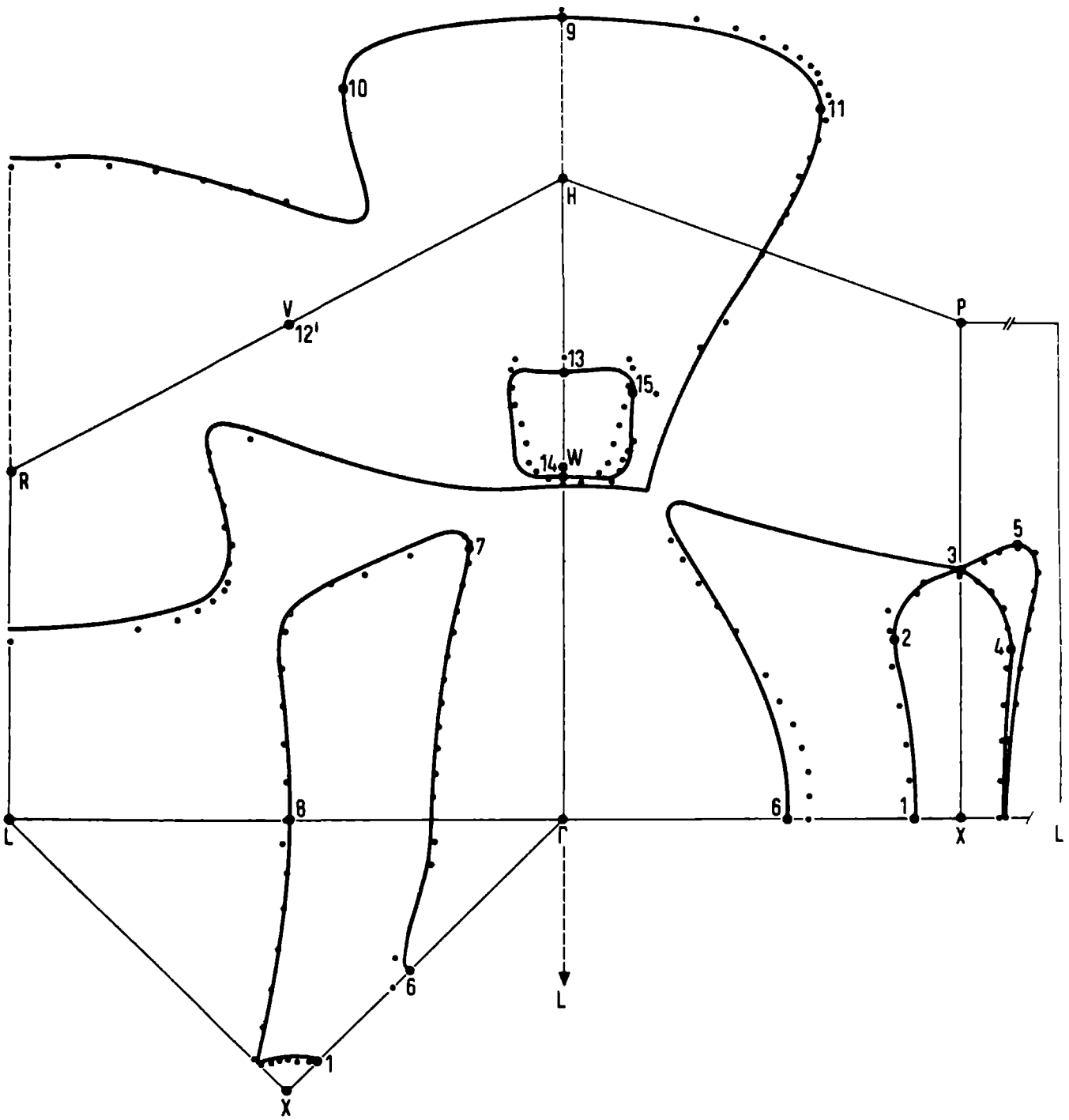

Fig. 1. Cross section of the FS with four symmetry planes from our RAPW calculation (solid lines) and from Craven's pseudo potential calculation (small dots). The Point 12' is the projection of point 12 on the LΓH plane (see Table 1 and 3).

Table 1.

Comparison between RAPW fitted, plane wave calculated and experimental semi calipers.

Zone [a]	Caliper	RAPW[b,c,d]	RPW[e]	Exp.[f]
3,1 (1)	$(\frac{1}{2} - k_x)2^{\frac{1}{2}}$	79	80	80
3,2 (2)	$(\frac{1}{2} - k_x)2^{\frac{1}{2}}$	117	129	121
3,3 (3)	k_z	456	449	456
3,4 (4)	$(k_x - \frac{1}{2})2^{\frac{1}{2}}$	87	85	91
4,5 (5)	k_z	500	496	496
4,7 (6)	$k_x 2^{\frac{1}{2}}$	398	440	400
4,10 (7)	k_x	172	166	172
4,1 (8)	$1 - k_x$	505	504	505
5,1 (9)	$k_z - a/2c$	566	583	566
5,4 (10)	k_x	398	400	396
5,5 (11)	$k_x 2^{\frac{1}{2}}$	465	468	459
5,6 (12')	$\frac{1}{2} - k_y$	335	349	337
6,1 (13)	k_z	828	858	
6,2 (14)	k_z	634	623	
6	central height	194	235	196 ± 2[g]
6,3 (15)	$k_x 2^{\frac{1}{2}}$	124	123	123

[a] The numbering between paranthesis is that of Fig. 1 and the other numbers are those of Table 3.

[b] The values are in units 10^{-3} c.u..

[c] This work.

[d] Mean abs. deviation between RAPW and exp. value: 2. Largest abs. deviation between RAPW and exp. value: 6.

[e] Ref. [6].

[f] Ref. [1].

[g] P. Kolling, Magneto Accoustic Effect, private communication.

α_4 and α_5 (Fig. 2). For our calculations we have chosen E_F = 1.60 c.u. The quality of the fit is very good (Table 1) and for only two points significantly beyond experimental error. This discrepancy will be discussed later on. (The experimental error in the RFSE measurements of [3] is less than 1%, unless stated otherwise explicitly).

We estimated the total error in our calculated k-values (where we traverse the Fermi surface more or less perpendicular), caused by the finite number of APW's (about 120), by the truncation of the l-sum at l = 5, by neglecting the interactions among the states with the higher zeroth order energies ($k_i^2 > 7$ c.u.), and by numerical interpolation procedures and rounding-off errors of the computer, to be less than .0005 c.u.

Among the spin-orbit coupling parameters, β_1 appears to be the only one which is important for the FS. Its value is mainly determined by the sixth zone around W.

The choice of E_F forms a peculiar problem in the sense that the quality of the fit turns out to be very insentive for the choice of E_F as is demonstrated by Table 2. Fig. 2 shows the fitted α_1 and the "empty potential" values of α_1 as a function of E_F with fixed β_1 = .24. Note the near linearity of the fitted α_1. This linear behaviour can be understood from the "on the

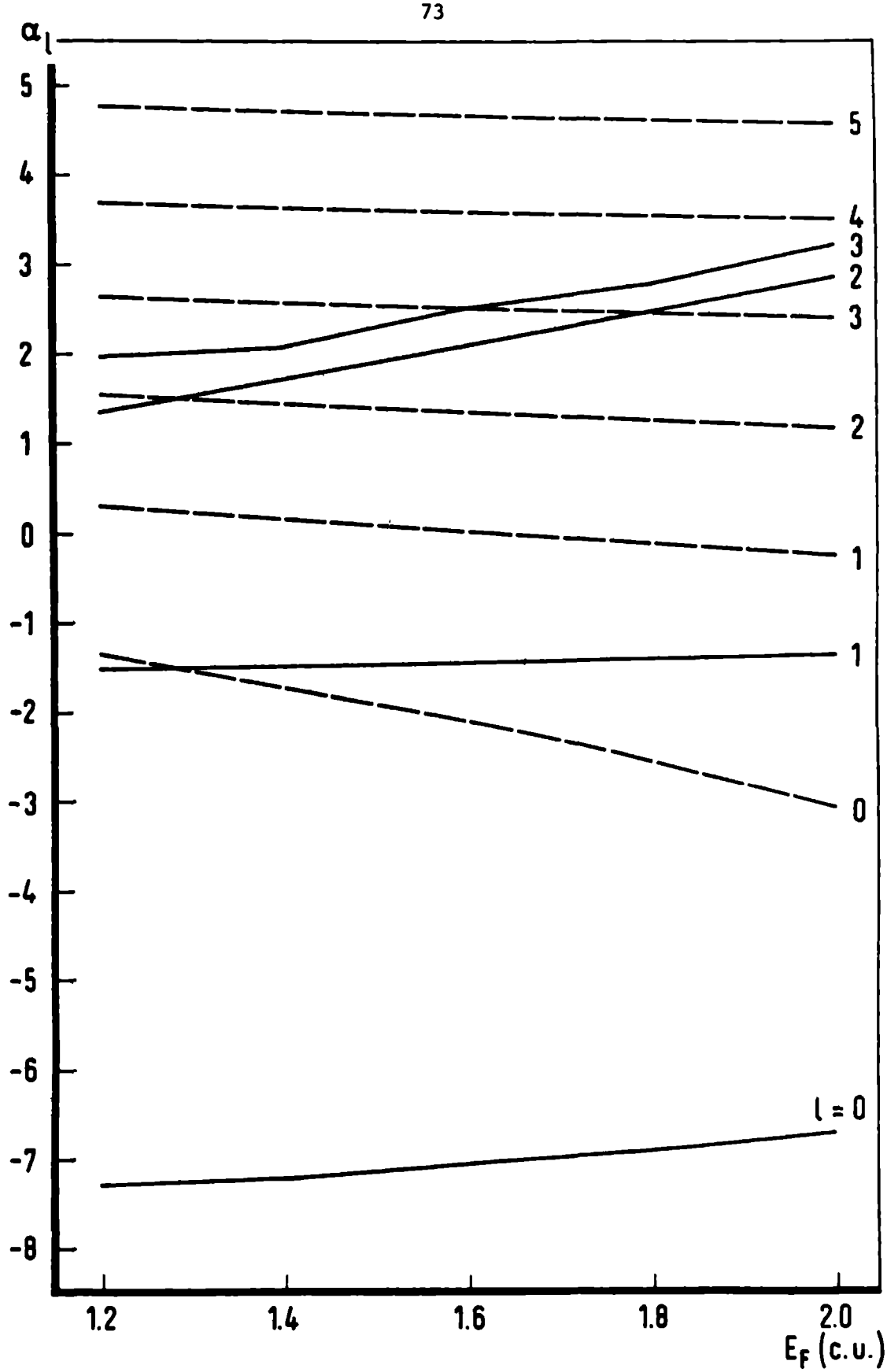

Fig. 2. The fitted (solid lines) and empty potential values (broken lines) of the logarithmic derivatives α_l as a function of E_F.

Table 2.

Quality of the fit and the values of the parameters as a function of E_F.

E_F[a]	m.a.[b] deviation	largest[b] deviation	α_o	α_1	α_2	α_3	β_1	η_o[c]	η_1	η_2	η_3	Z_F[d]
2.00	3	8	-6.73	-1.36	2.84	3.20	.24	.4572	.5331	- .1440	- .0120	.80
1.80	3	6	-6.92	-1.40	2.47	2.78	.24	.6040	.6530	- .0963	- .0040	1.31
1.60	2	6	-7.06	-1.450	2.07	2.52	.24	.7548	.7846	- .0522	.0001	1.813
1.60[e]	2	6	-7.15	-1.480	2.05	3.52	.20	.7593	.8021	- .0510	- .0075	1.820
1.60	3	6	-6.99	-1.474	2.08	3.06	.00	.751	.799	- .053	- .004	1.82
1.40	2	6	-7.23	-1.480	1.71	2.07	.24	.9155	.9111	- .0174	.0032	2.25
1.20	3	6	-7.31	-1.525	1.34	1.96	.24	1.0828	1.0548	.0096	.0028	2.75

[a] In units c.u.

[b] Mean absolute deviation of the RAPW values from the experimental ones of the semi calipers from Table 1; unit 10^{-3} c.u.

[c] The phase shifts η_l are calculated from α_l using formula (4).

[d] The Friedelsum Z_F is calculated using formula (5).

[e] With these values of E_F, α_1 and β_1 the whole FS of white tin has been calculated.

Fermi sphere" approximation [9] and the slopes can be related to muffin tin radii S_1 for which the E_F-dependence of α_1 vanishes [12,13]. An extensive discussion concerning the problem of the choice of E_F and the behaviour of α_1 and the Friedel sum as a function of E_F can be found elsewhere [2,14,9,12]. We feel that the Friedel sum as a function of E_F is an important quantity, since it is a curve of constant FS. We believe that any muffin tin potential, constructed from first principles, should end up with a Friedel sum lying on this curve.

3. Comparison with RFSE.

Once the parameters α_1 and β_1 have been fitted to the selected set of points on the FS we can calculate the whole FS and make a comparison with RFSE and other experiments. A large number of check points, cross sections and projections of the FS have been calculated. The projection of the FS on a certain plane with normal $\vec{n}$ is defined as the collection of projections of those points of the FS for which $\vec{v} \cdot \vec{n} = o$, $\vec{v}$ is the Fermi velocity and $\vec{n}$ is the normal to that plane. Table 3 shows a listing of calculated points with $\vec{v}.\vec{n}_1 = \vec{v}.\vec{n}_2 = o$, $\vec{n}_1$ and $\vec{n}_2$ being the normals to two of the main symmetry planes (100), (110) and (001). Table 4 shows a large

Table 3.

Calculated coördinates of points of the FS with $\vec{v}.\vec{n}_1=\vec{v}.\vec{n}_2=0$, $\vec{n}_1$ and $\vec{n}_2$ are two of the directions [100], [110] and [001]. Unit 10^{-3} c.u.

Zone	Point[a]	k_x	k_y	k_z	Zone	Point	k_x	k_y	k_z
3	1	444	444	0	5	1	0	0	1487
	2	417	417	330		2	380	0	1106
	3	500	500	456		3	0	0	614
	4	562	438	300		4	398	0	1350
4	1	495	0	0		5	329	329	1310
	2	239	0	0		6	500	165	920
	3	195	0	535		7	208	410	1145
	4	500	500	460		9	357	0	1140
	5	571	429	501		10	99	99	609
	6	141	141	583		11	150	0	611
	7	281	281	0		13	395	195	1147
	8	554	446	0	6	1	0	0	828
	9	129	129	565		2	0	0	634
	10	172	0	503		3	88	88	785
	11	290	260	0					

[a] See also Ref. [1].

number of check points. The indication of the angle in the RFSE measurements is taken from the directions [100], [110] and [100] respectively for the a-, b- and c-measurements. The agreement between experiment and calculation is excellent: mean absolute deviation of .002 c.u. and a largest deviation of .010 c.u. on about 60 points.

Fig. 3 to 11 show all calculated and/or experimental projections in three symmetry planes for zone 3 to 6. We shall use the following conventions:

a) $\Gamma \equiv (0, 0, 0)$ origin in $\vec{k}$-space

b) symmetry points of the Brillouin zone are indicated with capital letters, whereby we will follow the usual convention (see for example Fig. 5 of [1]). The same convention will be used for the labeled points of the FS from Table 3.

c) the calculated projections are drawn with heavy solid lines, the not calculated ones with heavy broken lines.

d) the RFSE measurements are indicated with thin broken lines and small dots. Orbits with a centre of inversion, as for example a3, b1 and b2 in Fig. 3 are plotted from that centre; orbits without a centre of inversion, as for example 2xa5, 2xb3 and 2xb4 in Fig. 3, are drawn with the aid of a "tangent construction". "Cut-off in $\vec{k}$-space" orbits[1], as for

Table 4.

Comparison of RFSE measured semi calipers of [1] and the RAPW calculated values (10^{-3} c.u.).

Zone	RFSE		RAPW	Remarks	Zone	RFSE		RAPW	Remarks
	Resonance	$\Delta k^{exp}/2$	$\Delta k^{calc}/2$			Resonance	$\Delta k^{exp}/2$	$\Delta k^{calc}/2$	
3	a 1(0°)	59.0 ± 1.5	59	Fig. 4, break	5	a12(0°)	337	335	Fig. 8,10
	a 3(0°)	66.0 ± 1.5	65	Fig. 3a, 4		a15(0°)	395	398	Fig. 8,10
	a 5(0°)	93 ± 2	92	Fig. 3a, 4		c 3(0°)	396		Fig. 10
	b 1(0°)	77.0 ± 1.0	74	Fig. 3b, 4		a14(0°)	359	357	Fig. 8
	b 2(0°)	80.3	79	Fig. 3c, 4		a10(0°)	329	328	break
	b 4(0°)	121	117	Fig. 3c, 4		a37(90°)	162	163	Fig. 8
	b 2	119		max [110]a		a37	171	171	max [001]
	b 4	99	98	min [110]		a36(90°)	189	190	Fig. 8
	b 3(0°)	90.7	87	Fig. 3b, 4		b13	190		max [001]
	b 1	88		max [110]		a22	566	567	max [001]
	b 3	82	81	min [110]		a33(90°)	250	252	Fig. 8
	b 3(90°)	456	456	Fig. 3b		a29(90°)	424	426	cut off orbit
						a30(59°)	459	460	Fig. 8
4	a 7(0°)	172	172	Fig. 5,7		a34(59°)	459		½(a34 + a22)
	a 9(0°)	292	290	Fig. 5,7		a22(59°)			
	a 8(0°)	271	275	Ref. [16]		b 6(90°)	165	166	Fig. 9
	a20(0°)	505	505	Fig. 5,7		b 6	169	170	max [001]

Table 4 (continuation).

	a18(0°)	475	476	Ref. [16]	13(90°)	180	180	Fig. 9
	a16(0°)	446	446	Ref. [16]	15(0°)	410 ± 10	415	Fig. 9
	a19(0°)	488	488	Fig. 5, 7	16(0°)	459	465	Fig. 9, 10
	a27(90°)	535	535	Fig. 5	c 3(45°)	462 ± 6		Fig. 10
	a25(90°)	586	583	Fig. 5	b27(90°)	440	439	Fig. 9
	a21	588		max [001]	c 9(0°)	653 ± 8	643	Fig. 10
	a25	558	559	min [001]	c11, c2	642 ± 8		Fig. 10
	a28(90°)	503	500	Fig. 5	c19	500		Fig. 10,
	b14(0°)	400	398	Fig. 6, 7				½Δk [100]
	b20(0°)	629	630	Fig. 6, 7	c19	201 ± 5	205	½Δk [010]
	b19(0°)	570	569	Fig. 7	c19	750		Fig. 10, p.A,
	b23(90°)	496	500	Fig. 6				½Δk [100]
	c21	326	328	min [100]	c19	145 ± 5	145	½Δk [010]
	a19, c1			Fig. 7,	c19	800		Fig. 10, p.B,
	a 7	1000		ΓL ≡ 1,000				½Δk [100]
	c 5(0°)	524	524	Fig. 7	c19	131 ± 5	130	½Δk [010]
6	a40(47°)	124	122	Fig. 11a	6 b 5(21°)	130	131	Fig. 11b
	a40(73°)	101	99	Fig. 11a	b 5(29°)	139	139	Fig. 11b
	a40(90°)	102	100	Fig. 11a	b33(56°)	124	122	Fig. 11b
	b 5(0°)	123	124	Fig. 11b, 11c	b33(90°)	102	100	Fig. 11b

Table 4 (continuation).

5,6	a31(90°)	294 ± 4	290	a36 + a40[b]	4,6	b24(90°)	604 ± 10	601	b23 + b33
4,6	a24(90°)	605 ± 9	600	a28 + a40	5,6	c 4(0°)	481 ± 6	478	c 3 + 6th
5,6	a23(90°)	661 ± 10	663	a37 + a28					zone - 20
5,6	b25(90°)	531	≈ 530	≈b27 + b33					

[a] With "max [110]" we mean the maximum value of the component of $\Delta k^{exp}(\theta)/2$ in the direction [110] for $\theta \neq 0°$.

[b] A lot of sum orbits has been measured [1]. For example the cubic shape of the sixth zone makes this piece of the Fermi surface very suitable for generating "current sheets" in the bulk of the sample, thus making sum orbits possible. We remark that often it happens that a caliper, which can not be measured itself directly because of the shape of its orbit, can be measured as a sum orbit.

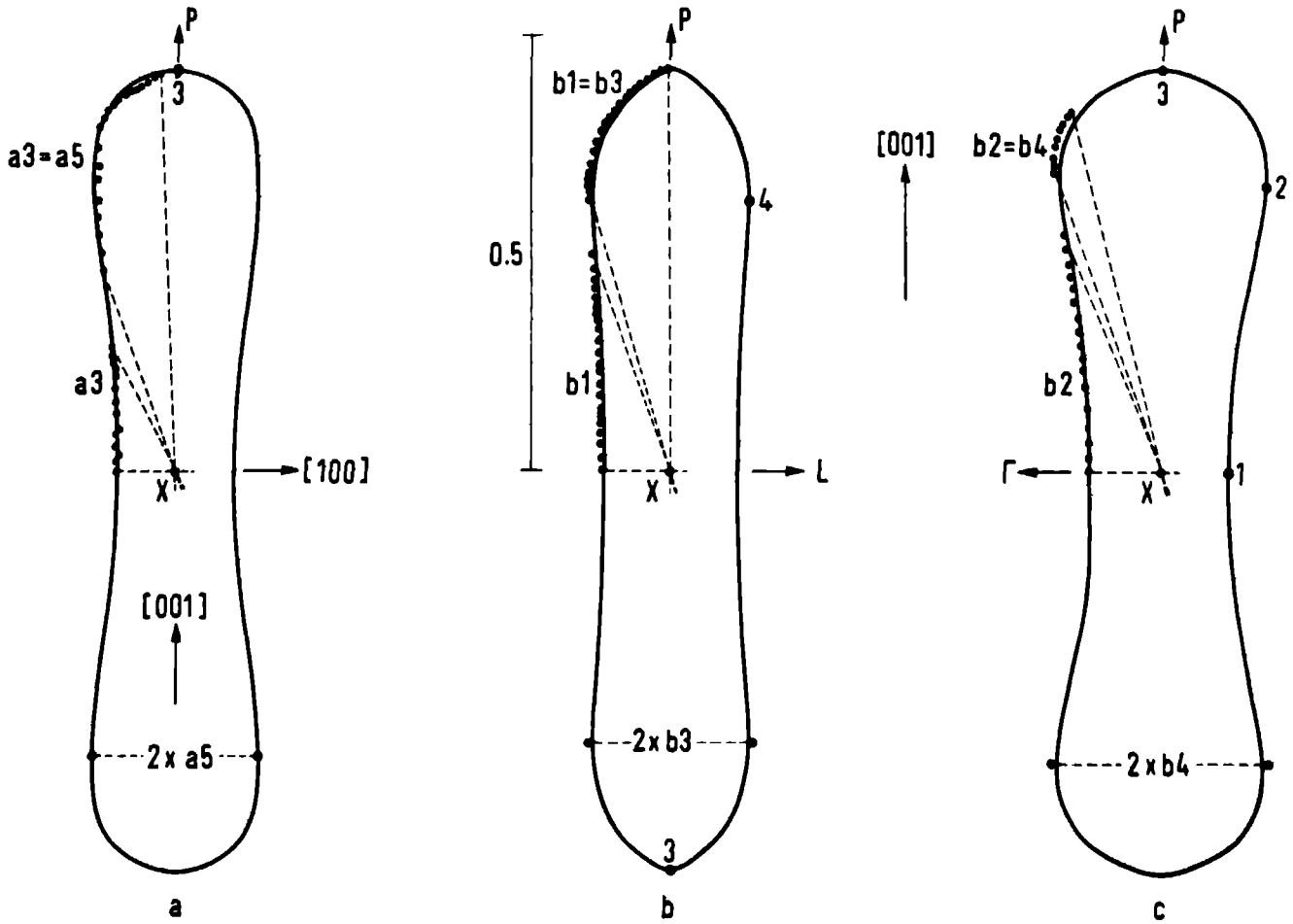

Fig. 3. Projection of the third zone: on (010) (a), on (1$\bar{1}$0) (b and c).

example 2xa29 and 2xa30 in Fig. 8 are incidentally indicated.

Now we will discuss all projections in detail.

Third zone.

Projection on (010), Fig. 3a.

From the known shape of the third zone we expect in the [100] direction a central minimum semi caliper and a non central maximum one which merge for large angles. These expectations are confirmed by a3 and a5. a5 is indicated only by a single point in the figure. The consistency between RFSE and RAPW is good.

Projection on $(1\bar{1}0)$, Fig. 3b, 3c.

The projection on $(1\bar{1}0)$ consists of two figures: the cross section of the third zone with the plane LXP and ΓXP respectively. Again there are, just like in Fig. 3a, two extrema in [110] which is consistent with the measurements b1 and b3 in Fig. 3b, respectively b2 and b4 in Fig. 3c.

At large angles there is a systematic discrepancy between RAPW and b1 and b2. The same discrepancy is shown by b14 and b23 in Fig. 6 and by b29, b30 and b31 in Fig. 9. These all are just those measurements which have been measured from a [110]-sample at large angles [1]. Therefore it seems to be probable, that these

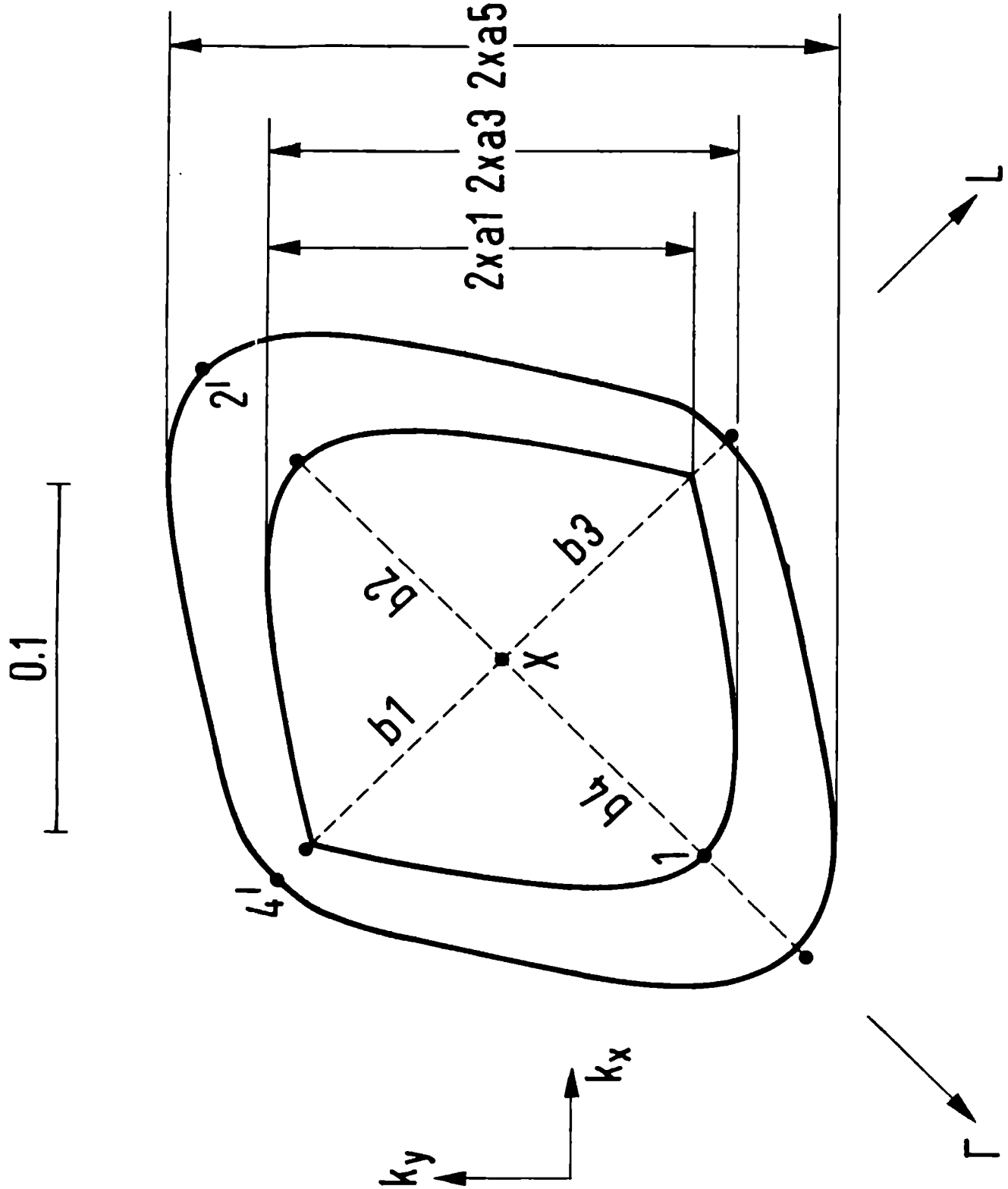

Fig. 4. Projection of the third zone on (001).

measurements ought to be corrected by .5° to 1° towards [001] in the plane (110).

Fig. 3b is the dHvA cross sectional area δ_3^1 (Table 5). Our calculated value agrees with the experimental one to within one per cent. The cross sectional area in Fig. 3c has not been detected in dHvA experiments.

Projection on (001), Fig. 4.

The smallest figure is the cross section with the k_z = o plane, its area is the dHvA oscillation δ_1^1 (Table 5). Our calculated area is 3.5 % greater than the experimental values. This means only about .001 c.u. in the semi calipers. 2xa1 and 2xa3 agree excellently with RAPW, while b1 and b2 are significantly larger than the RAPW dimensions. Such an inconsistency is also seen for the largest figure in Fig. 4. This figure is the projection of points of the FS from the neighbourhood of the δ_1^2 dHvA cross section for which RAPW and experiment agree within 1% (Table 5). The agreement between RAPW and 2xa5 is very good too. However b3 and b4 are significantly larger than RAPW. Unfortunately from the c-measurements no data are available for the third zone. For the discrepancy between RAPW and the experimental b1 to b4 we don't have a satisfying explanation. It seems to us that most probably the experimental b1 to b4 along [110] are systematically too large by about .002 c.u.

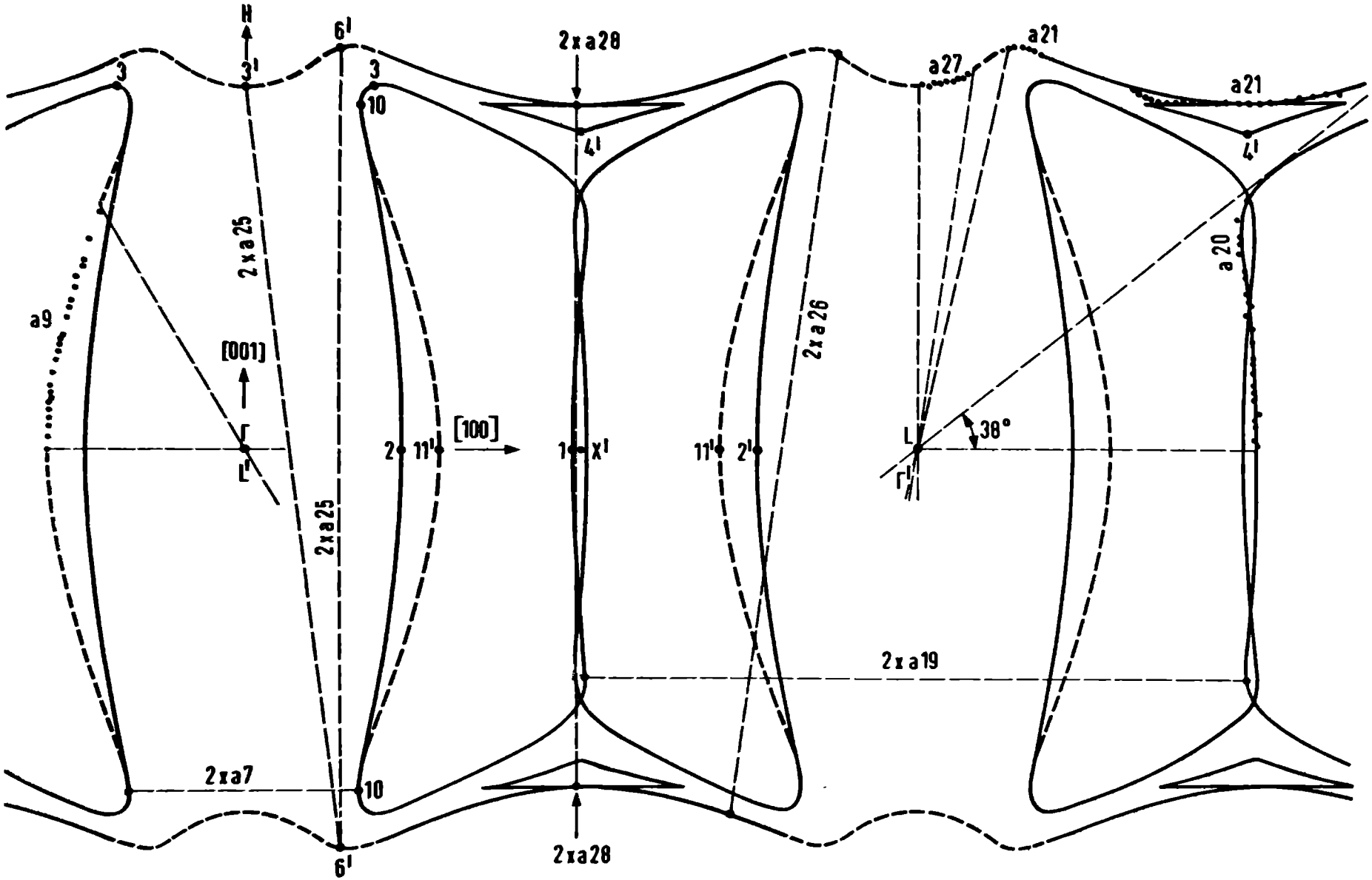

Fig. 5. Projection of the fourth zone on (010).

On the line XP the third and fourth zone are degenerated. This degeneration is removed by spin-orbit coupling. However the splitting remains very small: about .003 c.u. Consequently there remain sharp bends in the cross section of the third and the fourth zone with the k_z = o plane. Such sharp bends give rise to additional RFSE resonances: so called "breaks" [15]. For example 2xa1 is consistent with a break in the third zone δ_1^1 orbit (Fig. 4); 2xa18 and 2xa16 are consistent with breaks in the fourth zone ϵ_1^5 orbit (see Fig. 1 of Ref. [16]).

Fourth zone.

Projection to (010), Fig. 5.

The points 3 and 6 have been calculated; their projections corresponds with a27 and a25 along [001]. The interpolated curve 3'-6' of the projection has been estimated from the measurements a27 and a25. From the curve 10-11' the points 10 and 11' have been calculated and they are consistent with a7 and a9 along [100].

The curve 2-10 can not be measured directly with RFSE. However the curve 2-10-3-1 is the dHvA cross section ϵ_1^1 (Table 5) and, keeping in mind the consistency between RAPW and a20, a19, a27, a7 and the cross section area ϵ_1^1, we may conclude that the points on the curve have been determined to within .002 c.u. along their normal

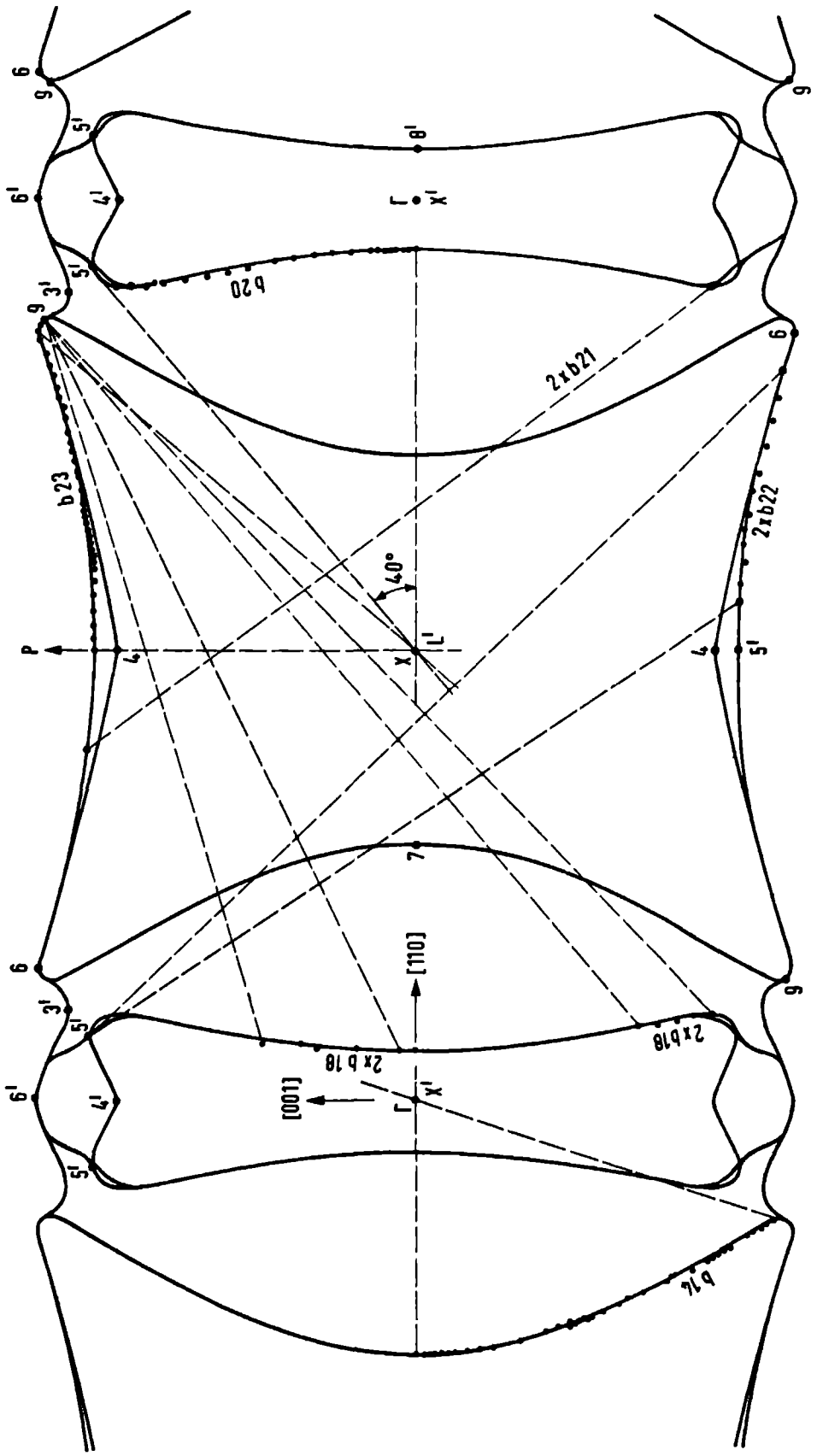

Fig. 6. Projection of the fourth zone on (1T0).

component.

The consistency between RAPW and a21 is less rigourous.

The "cut-off in k-space" orbit a28 is in good agreement with RAPW.

Projection to $(1\bar{1}0)$, Fig. 6.

The central semi calipers b14, b20 and b23 are in good agreement with RAPW, especially along the symmetry directions. For the larger angles the same systematical error of about $.5^{\circ}$ as for b3 and b4 in the third zone is seen (see comments on the third zone). The interpretation of b22 and b21 is rather complicated. b22 seems to be a normal RFSE resonance. (For sake of clarity we have taken 5' as origin for the b22 calipers.) b21 is caused by a drastic change of the shape of the orbit in $\vec{k}$-space, going along the direction of the magnetic field.

The curve 4'-5'-8' is the dHvA-area ϵ_3^1 (Table 5). The RAPW area is 2.5% smaller than the experimental value. This means only .002 c.u. in the direction [110], which is well within the experimental error in b20.

The curve 7-6-4 is a dHvA cross section, which has not been measured experimentally however. The RAPW value is .788 c.u.

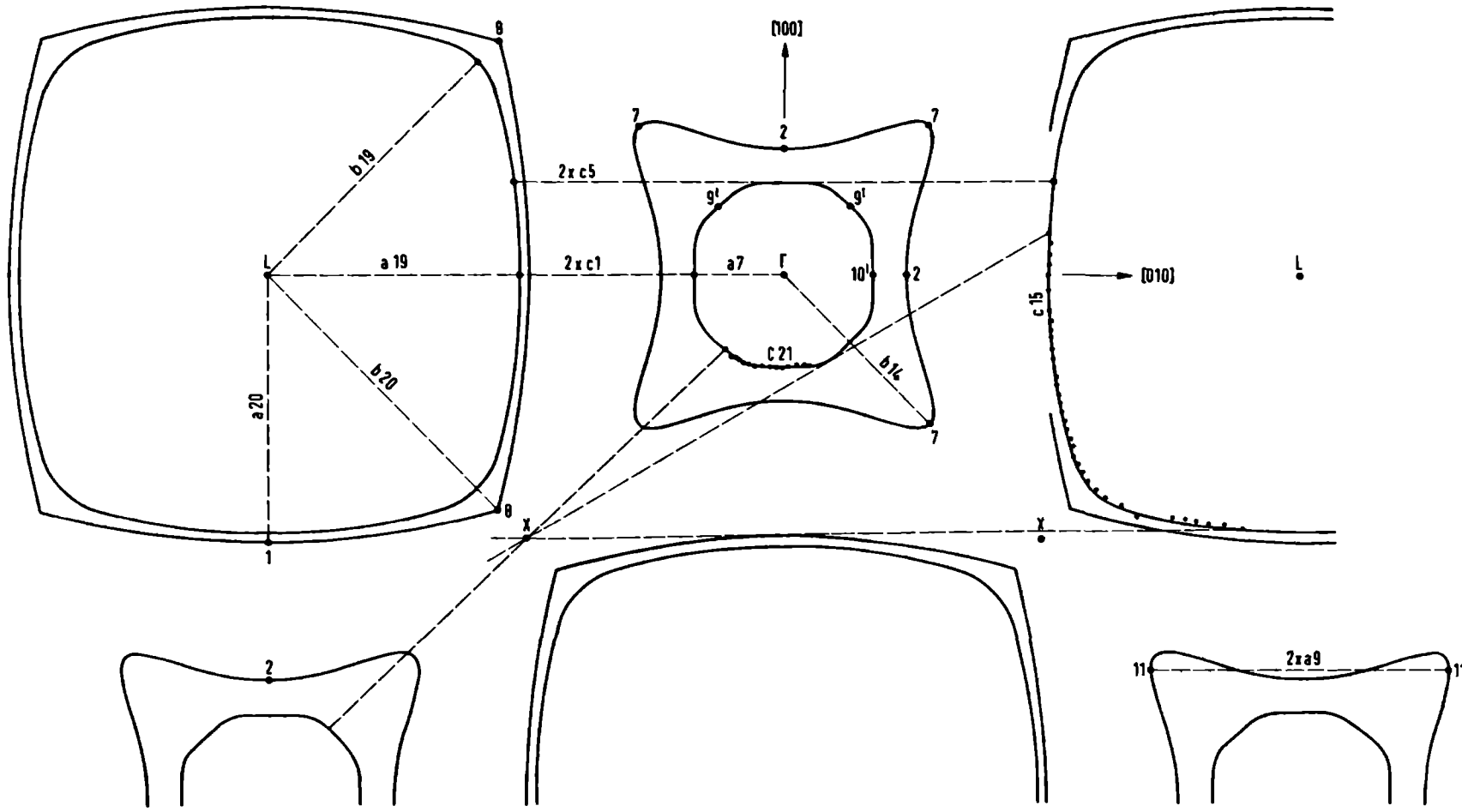

Fig. 7. Projection of the fourth zone on (001).

Projection to (001), Fig. 7.

The consistency between RAPW and the RFSE measurements c1, c5, c15 and c21 is nearly perfect. Further still some other points of the projection curves have been measured in the (010) and $(1\bar{1}0)$ samples as indicated in the figure.

The curves 1-8 and 2-7 are cross sections with the k_z = o plane and their areas correspond with ϵ_1^5 and ϵ_1^2 respectively (Table 5).

The points 9 and 10 lie in the neighbourhood of the dHvA cross section with the plane k_z = .52 c.u., which has not been detected experimentally. The RAPW value is .110 c.u.

The specific curvature around point 11 gives rise to a special RFSE resonance [16] (Table 4).

Fifth zone.

Projection to (010), Fig. 8.

The agreement of RAPW with a33, a34, a37, a38, a36, a29 and a15 is perfect, just as for the limiting angles of a22: 37^o and 59^o. a14, a29 and a30 are consistent with "cut-off" resonances. At the limiting angle 59^o the relation 2xa30 = a34 + a22 should hold (See Table 4).

a12 and a14 show some larger experimental inaccuracy, nevertheless they agree reasonably well with RAPW. The

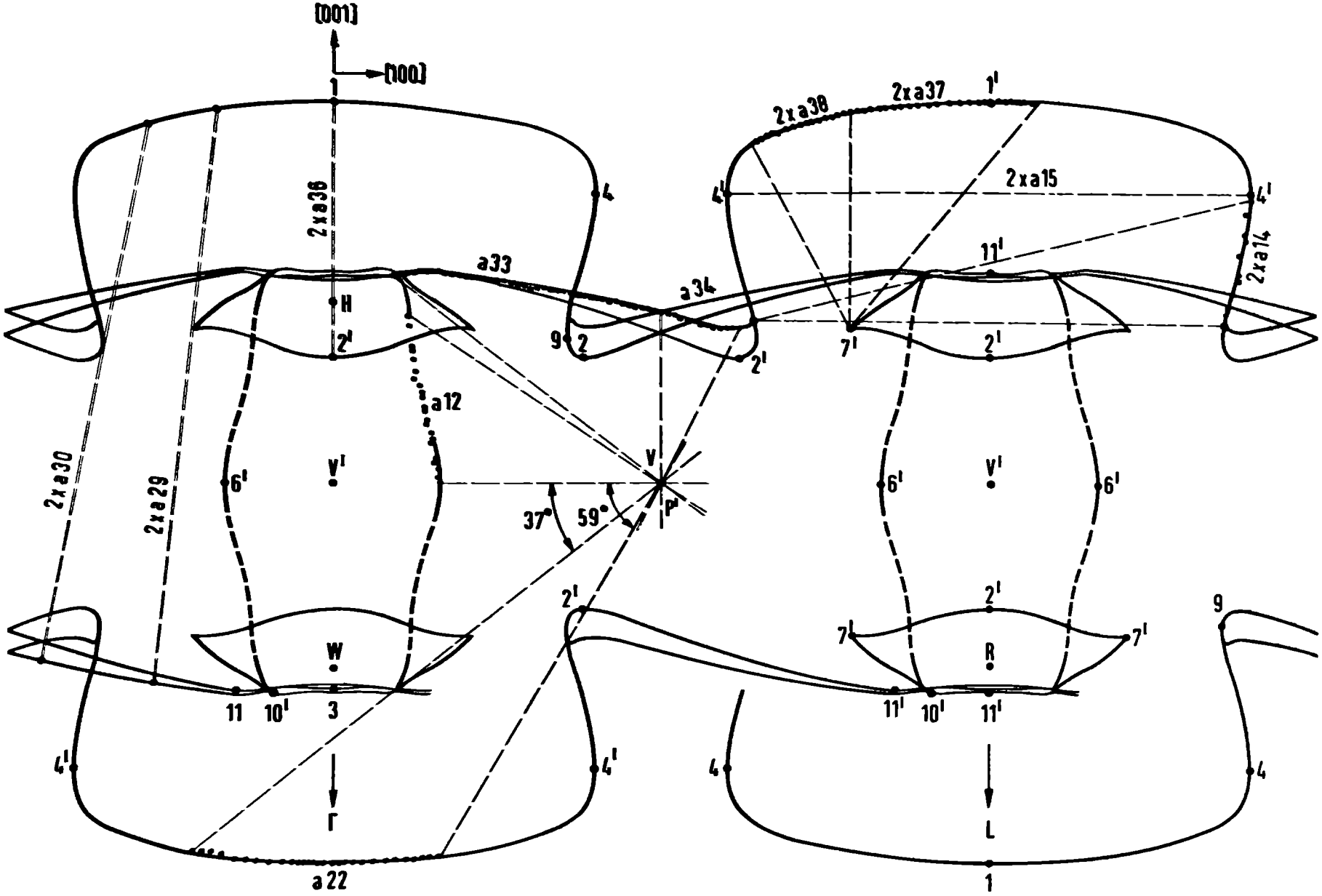

Fig. 8. Projection of the fifth zone on (010).

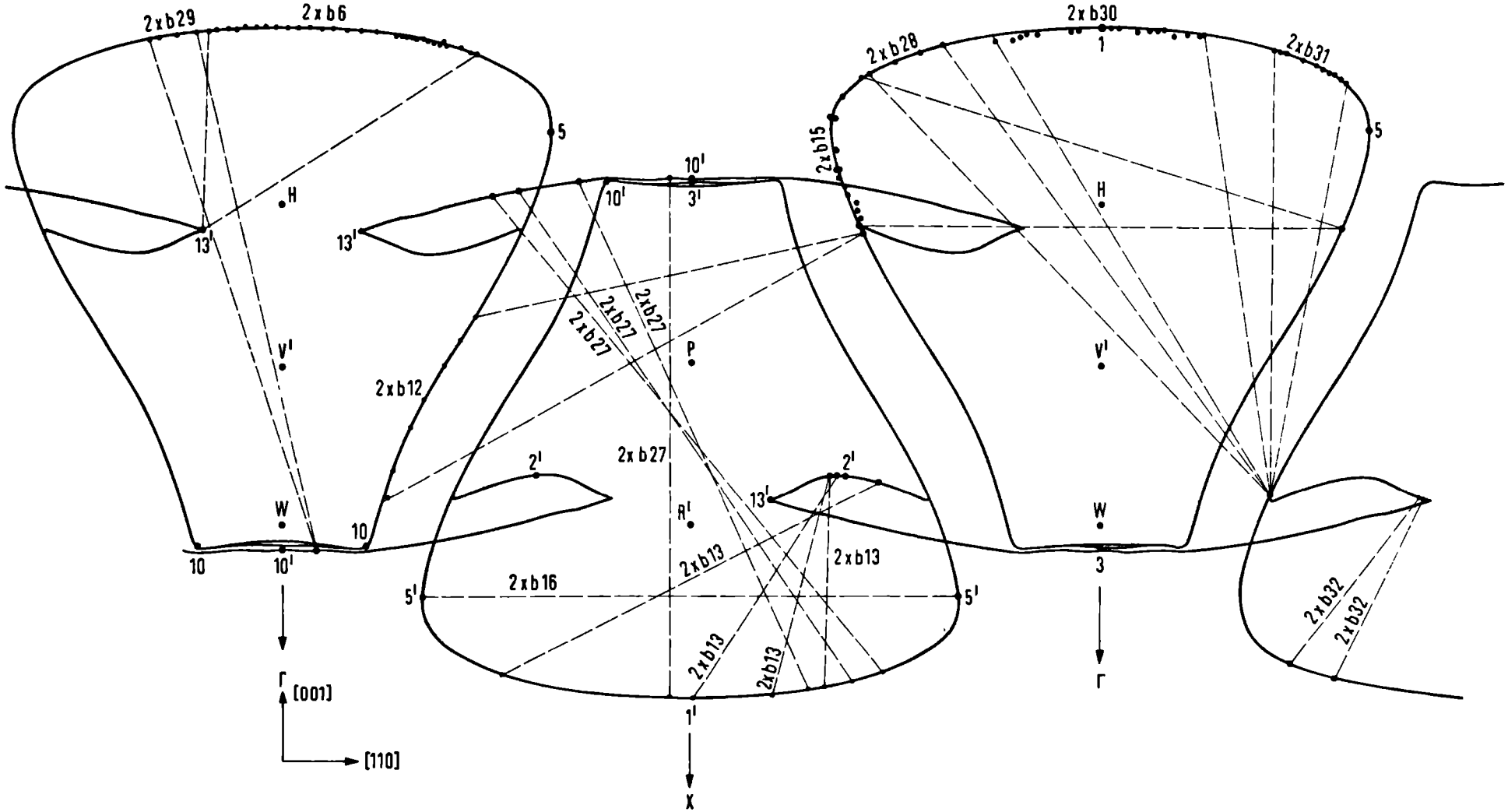

Fig. 9. Projection of the fifth zone on (1$\bar{1}$0).

not calculated part of the curve 6'-10' has been estimated from a12.

Projection to $(1\bar{1}0)$, Fig. 9.

The consistency between RAPW and b6, b32, b13, b27 and b31 is perfect. b16 and the cut off orbits b15 and b12 agree reasonably with RAPW. The interpretation of b30 seems to be reliable (see comments third zone), that of b28 between 70^{o} and 80^{o} is not very clear. The interpretation of the non central orbits b13, b16, b32, b27 and b29 requires a tangent construction; this has been done for a limited number of points.

The curve 1-5-10-3 is the dHvA cross section with the plane $k_x = k_y$. The area corresponds with π_2^3 (Table 5).

Projection to (001), Fig. 10.

The projection consists of two curves: 4'-5' which has been calculated entirely, and the projection of the tubes, connecting the pears 1-1, 9'-6, which has been calculated partly. The RAPW curve 4'-5' is in good agreement with c3, a15(0^{o}) and b16(0^{o}). The curve 9'-6 is determined experimentally by c9, c19, c11 and a12(0^{o}). c19 is consistent with the RAPW curve. For an additional comparison the points A and B have been also calculated (Table 4).

Further, some points from c2, c6, c10, c17 and c20

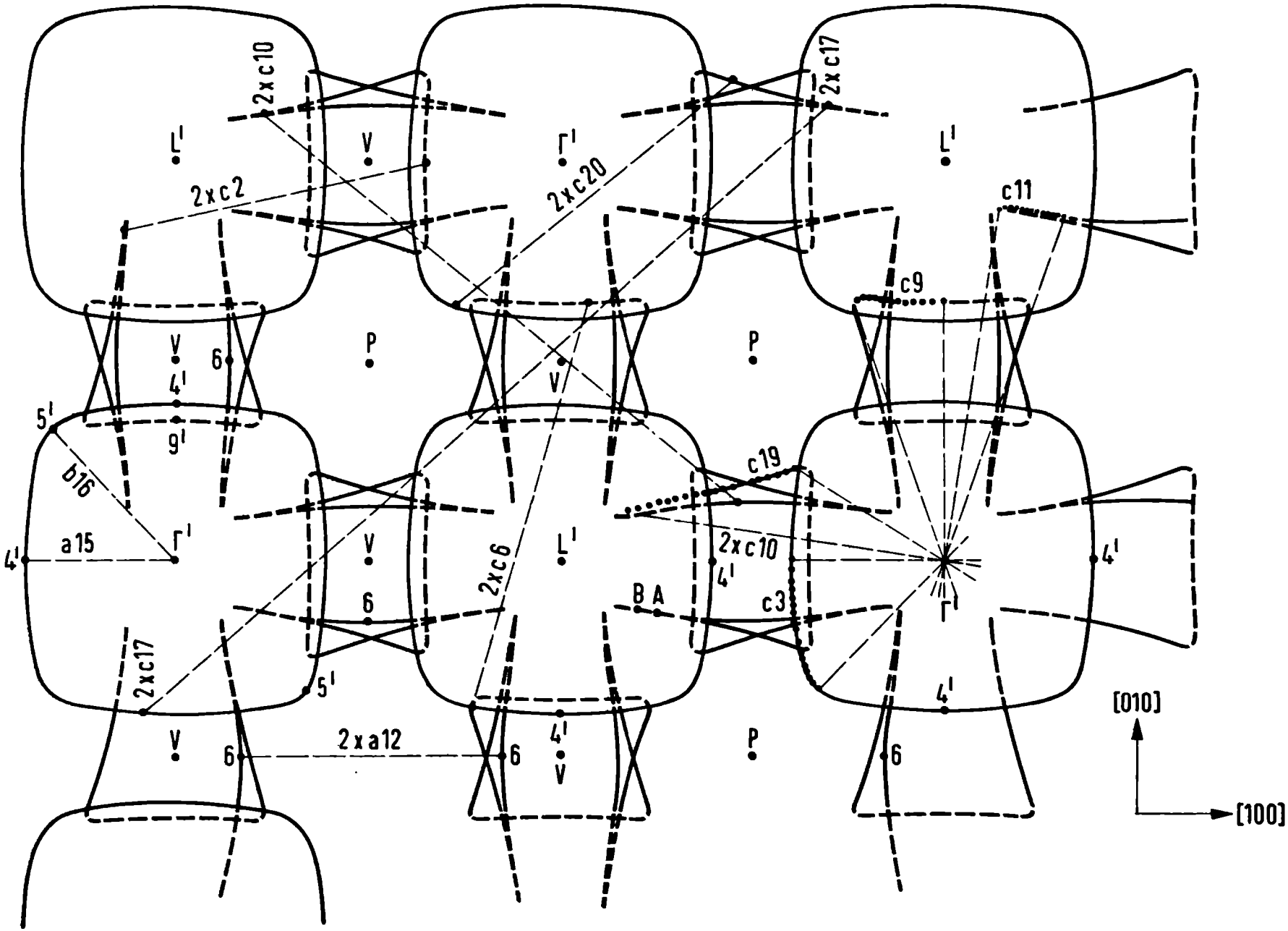

Fig. 10. Projection of the fifth zone on (001).

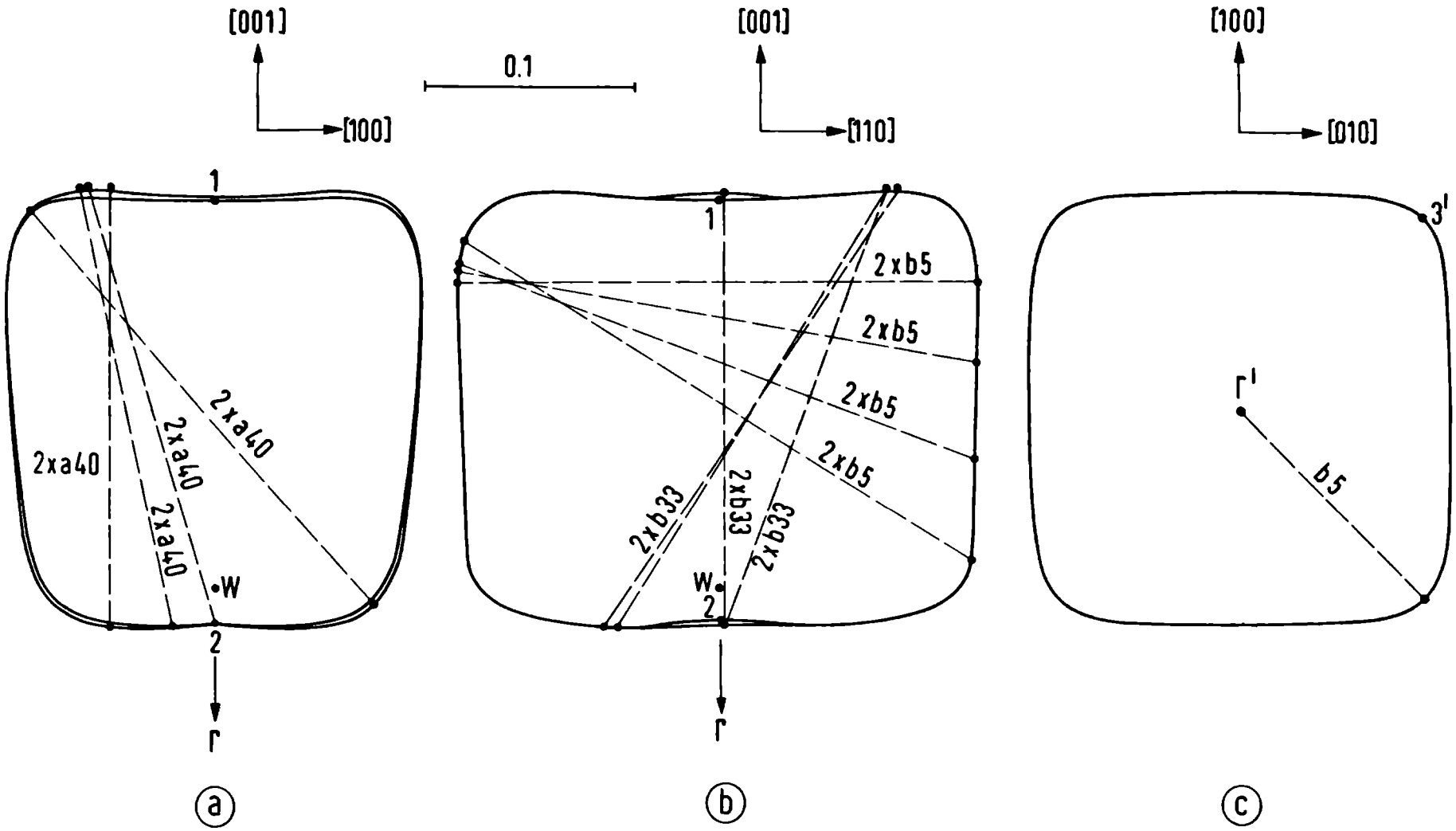

Fig. 11. Projection of the sixth zone: on (010) (a), on (1$\bar{1}$0) (b) and on (001) (c).

have been indicated in the figure.

The curve 4'-5' consists of the projection of points, which are lying in the neighbourhood of the dHvA cross section π_1^7 (Table 5).

Sixth zone.

Projection to (010), Fig. 11a.

a40 is in good agreement with our calculation. The measurements should be drawn with the aid of a tangent construction. It is not clear why the dimension in the [100] direction has not been measured with RFSE.

The inner curve is the central dHvA cross section with the (010) plane and the area corresponds with τ_2^1 (Table 5). From the figure it is obvious, that there should be another, non-central dHvA cross section (see note at Table 5).

Projection to $(1\bar{1}0)$, Fig. 11b.

The agreement between RAPW and b33 and especially b5 is good. These measurements require a tangent construction. The RAPW dimensions in the [001] direction are systematically smaller than those, which follow from a40 and b33. The explanation for this might be sought in the fact, that because of the cubic shape of the sixth zone, a small error in the orientation of the sample causes appreciable errors in the RFSE

measurements.

The inner curve of the projection is the central dHvA cross section with the $(1\bar{1}0)$ plane. The area corresponds with τ_3^1 (Table 5).

Without spin-orbit coupling the sixth zone is degenerated with the fifth zone on the line $k_x = k_y$ through W ($k_z = .650$). The spin-orbit coupling parameter β_1 yields a splitting of about $\Delta k = .04$ c.u. on this line.

Projection to (001), Fig. 11c.

From the curve only one point has been measured: $b5(0^o)$. The curve consists of the projection of points, which are lying in the near vicinity of the dHvA cross section with the plane $k_z = .790$. The area corresponds with τ_1^1 (Table 5).

4. Comparison with dHvA data.

We have calculated a large number of dHvA cross sections to compare them with the experimental values of Stafleu [4] and Craven et al [5] (Table 5). The mean relative deviation of RAPW with both Stafleu and Craven is 1.5 per cent and the largest relative deviation is 4.5 and 3.5 per cent respectively. The error in the experimental values of Craven is "almost everywhere better than" 1 per cent. That is, the mean relative deviation is somewhat larger than the experimental error,

Table 5.

dHvA - areas[a].

Plane	Symbol[b]	Experimental		Calculation	
		Stafleu, et al.[c]	Craven, et al.[b]	RAPW[f]	RPW[g,h]
ΓXL	δ_1^1	14.0 ± .15	14.0	14.5	14.0
(k_z = .320)	δ_1^2	26.6 ± .25	26.4	26.7	26.6
(k_y = .500)	δ_2^1	127 ± 2.5	129	127	127
LXP	δ_3^1	137 ± 2.5	137	136	134
ΓXL	ϵ_1^2	286 ± 4	277	274	280
LXP	ϵ_3^1	208 ± 4	209	203	208
LΓH	ϵ_1^1	278 ± 4	269	272	270
(k_z = .340)	ϵ_1^4	860 ± 20	840	856	847
ΓXL	ϵ_1^5	900 ± 20	914	934	923
ΓXL	B		1094		
ΓXP	π_2^3	564 ± 8	551	562	554
(k_z = 1.340)	π_1^7	560 ± 8	554	566	560
(k_y = .500)	π_2^1 [d]	170 ± 2	170	173	169
(k_y = .410)	π_2^2		168	171	
(k_z = .920)	π_1^5	441 ± 9	432	425	438
LΓH	τ_2^1 [e]	35.9 ± .4	36.5	35.6	37.1
(k_y = .050)	τ_2^1			36.2	
ΓXP	τ_3^1	46.6 ± .9	47.8	46.8	46.9
(k_z = .790)	τ_1^1	36.4 ± .4	36.2	37.4	36.2

Table 5 (continued).

[a] Areas in unit $10^{-3}(\Gamma L)^2$.

[b] Reference [5]; inaccuracy "almost everywhere better than 1%".

[c] Reference [4] (Note: on page 683; A = .0829 F should be A = .0817 F).

[d] π_2^1 and π_2^2 should be interchanged in Ref. [5].

[e] Our RAPW calculation shows a non central τ_2^1 with about the same dA/dk_y as the central one. In fact Stafleu, 1966, [private communication] did measure those two dHvA frequencies with the aid of a torsion method: from field rotation diagrams and direct measurements he determined the frequency difference to be 2%, which is in perfect agreement with our calculations.

[f] Mean rel. dev. $(A_{RAPW}-A_{Stafleu})/A_{Stafleu}$: 1.5%, largest dev. 4.5%.

Mean rel. dev. $(A_{RAPW}-A_{Craven})/A_{Craven}$: 1.5%, largest dev. 3.5%.

[g] Ref. [6].

[h] Mean rel. dev. $(A_{RPW}-A_{Stafleu})/A_{Stafleu}$: 1%, largest dev. 3.5%.

Mean rel. dev. $(A_{RPW}-A_{Craven})/A_{Craven}$: 1%, largest dev. 2%.

which is not entirely understandable, specially for the large areas. For example, if we suppose an uncertainty of .002 c.u. in the RAPW dimensions of the ϵ_1^5 orbit, then the uncertainty in its area will not be more than about .7 per cent. However the discrepancy amounts to 2 per cent. From an analysis of Craven's experimental results there appears a slight inconsistency in these measurements. Following Craven's interpretation along [001] the following should hold: $\epsilon_1^5 + B - 2\,\delta_1^1 \equiv 2.000$ c.u. However, substituting Craven's experimental values yields 1.980 c.u., suggesting that the values for both ϵ_1^5 and B are too small by 1 per cent. This correction would remove the above discrepancy by a great deal indeed.
This suggestion is also supported by a similar deviation for ϵ_1^4.

Further support for our suggestion is found in Stafleu's measurements [4] . He assigned his G_4 and G_1 oscillations to the ϵ_1^4 and ϵ_1^5 orbits respectively. The former agrees well with our calculation while the latter does not. Craven's discussion of his ϵ_1^5 and A measurements and the fact, that Stafleu performed his G measurements at rather high magnetic fields (30-35 kGauss, private communication) make it highly probable, that Stafleu's G_1 oscillation should be interpreted as Craven's A measurements, or at least as a mixing of Craven's A and ϵ_1^5 oscillations.

5. Comparison with other bandstructure calculations.

Earlier calculations are from Weisz (1966), Stafleu et al (1967) and Craven (1968). All of them used the Fourier transforms of the local pseudopotential as adjustable parameters.

Weisz [17] based his work on Gantmakher's RFSE measurements [18], which however are systematically too large [19, 3]. Therefore his interpolated FS deviates appreciably from the new measurements of [3].

Stafleu et al [4] based their calculations on their dHvA measurements, but they used a "few plane waves" scheme only, so their resulting calipers are not very accurate.

Craven [6] fitted the Fourier transforms to his accurate dHvA measurements [5] and he used about 50 plane waves. Therefore we think his calculations to be superiour to the former ones and we will compare with his results only (Table 1, Table 5 and Fig. 1). Though plane wave calculations by Craven agree very well with his dHvA data, his calculated calipers show deviations by up to .04 c.u. compared with the RFSE measurements of [3].

We believe the deviations of Craven's pseudo potential calculations from the RFSE measurements of [3] to be due to a wrong value of the Fermi energy mainly. We have performed [20] a pseudo potential fit to the

same 14 points of Table 1 using the Fermi energy as another independent parameter. The Fourier coefficients and the r.m.s. deviation of k showed a considerable dependence on the choice of E_F. The best fit has a r.m.s. deviation twice as bad as the best RAPW fit. Further results can be found elsewhere [20].

6. Conclusions.

We believe to have shown, that - remarkably enough - the parameters of the muffin tin potential can describe excellently the Fermi surface of a polyvalent, nearly free electron and rather anisotropic metal. The consistency between RAPW and the experimental data is of such a quality that we feel that the experimental accuracy is not yet sufficient to show the limits of the RAPW model. This partly is due to the fact that the deviation of the muffin tin model, i.e. the modulation of the potential between the muffin tin spheres, can be absorbed in the scattering parameters of the potential wells.

Further we believe to have been able to describe the linear dimensions of the Fermi surface of white tin to within .002ΓL, which is considerably better than the results of earlier interpolating calculations. Although of a complicated shape the Fermi surface of white tin is now one of the most accurately known among the polyvalent metals.

References.

[1] M.M.M.P. Matthey, M.A.C. Devillers and A.R. de Vroomen, accompanying paper.

[2] M.A.C. Devillers and A.R. de Vroomen, Phys. Letters, 30A, 159 (1969).

[3] M.M.M.P. Matthey and A.R. de Vroomen, Solid State Comm., 9, 1329 (1971).

[4] M.D. Stafleu and A.R. de Vroomen, Phys.Stat.Sol., 23, 675 (1967); 23, 683 (1967).

[5] J.E. Craven and R.W. Stark, Phys.Rev., 168, 849 (1968).

[6] J.E. Craven, Phys.Rev., 182, 693 (1968).

[7] T.L. Loucks, Augmented Plane Wave Method, W.A. Benjamin, Inc., New York, 1967.

[8] L.F. Mattheiss, Phys.Rev., 151, 450 (1966).

[9] M.A.C.Devillers and A.R. de Vroomen, Solid State Comm., 9, 1939 (1971).

[10] N.J. Coenen and A.R. de Vroomen, J.Phys.F: Metal Phys., 2, 482 (1972).

[11] J.A. Rayne, B.S. Chandrasekhar, Phys.Rev., 120, 1658 (1960).

[12] M.A.C.Devillers, Sol.State Comm., 11, 395 (1972) and erratum.

[13] O.K. Anderson, Phys.Rev.Letters, 27, 1211 (1971).

[14] M.J.G. Lee and V.Heine, Phys.Rev.B, 5, 3839 (1972).

[15] V.F. Gantmakher, Sovjet Phys. - JETP, 22, 734 (1966)

[16] M.M.M.P. Matthey and A.R. de Vroomen, Phys. Letters, 36A, 59 (1971).

[17] G. Weisz, Phys. Rev., 149, 504 (1966).

[18] V.F. Gantmakher, Sovjet Phys. - JETP, 17, 549 (1963); 19, 1366 (1963).

[19] A. Fukumoto and M.W.P. Strandberg, Phys. Letters (Netherlands), 23, 200 (1966).

[20] M.A.C. Devillers and A.R. de Vroomen, Phys. Rev. B, 4, 4631 (1971).

APPENDIX B.

A pseudo potential form factor for mercury.

J. Phys. F: Metal Phys., Vol. 3, November 1973. Printed in Great Britain. © 1973.

LETTER TO THE EDITOR

A pseudopotential form factor for mercury

M A C Devillers†, W H Young‡ and A R de Vroomen†

† Fysisch Laboratorium, Katholieke Universiteit, Nijmegen, The Netherlands
‡ School of Mathematics and Physics, University of East Anglia, Norwich NOR 88C, UK

Received 13 September 1973

Abstract. From accurate de Haas–van Alphen measurements one can deduce an unambiguous form factor for mercury. The calculated value of the specific resistivity of liquid mercury, based on this form factor, overestimates the experimental value. A correction factor $(m^*)^4$ is proposed which brings the calculated value of the specific resistivity into excellent agreement with the experimental one. The calculated volume derivative of the specific resistivity at the melting point agrees reasonably with the experimental value.

In the current literature there exists much confusion about the sign and magnitude of the pseudopotential form factor of mercury (Animalu and Heine 1965, Brandt and Rayne 1966, Bogle *et al* 1969, Evans *et al* 1969, Evans 1970, Jones and Datars 1971, Takeuchi 1971, see also Naguchi and Takeuchi 1973). The specific resistivity and related properties depend critically on the value of the form factor for q near $2k_F$ so there is need for a rather precise determination of the latter. Recently, accurate de Haas–van Alphen (dHvA) data (Poulsen *et al* 1971) have become available and these can be used for the experimental determination of some muffin tin parameters, for example the logarithmic derivatives $\alpha_l(E_F, R)$ in the APW scheme, R being the muffin tin radius, or alternatively the reduced phase shifts $\eta_l(E_F)$ of the muffin tin well. It is well established now (Devillers and de Vroomen 1971, Lee and Heine 1972) that band structure schemes based on the muffin tin model can be used very well to interpolate experimentally known Fermi surface geometry, that the resulting $\eta_l(E_F)$ are independent of the scheme being being used (APW, KKR or KKRZ) and that the parameters can be converted to a local form factor of some effective pseudopotential. We have used the APW scheme to fit η_0, η_1 and η_2 in a relative least squares procedure to the dHvA orbits $\alpha(1\bar{1}0)$, τ, τ', β and $\eta(111)$ of Poulsen *et al* (1971). From local pseudopotential arguments, which turn out to be not too bad for mercury, we may expect four local minima of the RMS deviation in parameter space, ie if V_{100} and V_{110} ($\simeq V_{111}$) is the correct solution of the band structure problem then the sets $\{-V_{100}, V_{110}\}$, $\{V_{100}, -V_{110}\}$ and $\{-V_{100}, -V_{110}\}$ should be rather good solutions too in first order approximation. Indeed we have found those four alternatives, albeit that two of them did not yield β arms in the X Brillouin zone face. In our opinion, on the whole the work of several authors should be classified as in table 1.

Alt-I and Alt-IV yield β arms only at the cost of large discrepancies with the α and τ orbits. As there is almost unambiguous experimental evidence for the existence of the β arms (open orbits in the magnetoresistance and cut off's in dHvA measurements) we are forced to exclude Alt-I and Alt-IV.

Table 1. Characteristics of the various alternative form factors of mercury

Notation	Sign of $\Gamma^{APW}_{(100)}$	Sign of $\Gamma^{APW}_{(110)}$	Main character of lens	Main character of T, X opening	Authors
Alt-I			p	s, d (no β arms)	Jones, class A; Evans
Alt-II		+	s, d	p	Jones, class B (?)
Alt-III			p	p	Jones class C; Animalu; Brandt
Alt-IV	+		s, p, d	s, d (no β arms)	

Between Alt-II and Alt-III the latter appears to be favoured rather strongly for the following reasons:

(i) The fit to the five areas, mentioned above, is somewhat better for Alt-III (1·5% RMS, which is about twice the experimental inaccuracy) than for Alt-II (2·2% RMS).

(ii) The agreement with magneto-acoustic calipers of Bogle *et al* (1969) is significantly better for Alt-III.

(iii) Better agreement with the experimental angular range of magnetoresistance open orbits and dHvA signals.

(iv) The right anisotropy of the α dHvA orbits in the field directions from $(1\bar{1}0)$ towards (111) (whereas Alt-II does not give any anisotropy!).

(v) In the free electron model the (100) Brillouin zone face acts like a mirror plane for the electron lens. But Alt-III yields an asymmetry: the electron lens is tipped 3° out of the (100) Brillouin zone face from (100) towards (111) and this seems to be confirmed excellently by recent cyclotron resonance measurements of Poulsen *et al* (1971); whereas the free electron like Alt-II gives only a slight asymmetry of about 0·5° in the wrong direction.

As for other metals (Devillers and de Vroomen 1971, Lee and Heine 1972) E_F is a weak parameter. The best fit was obtained for $E_F = 0{\cdot}30$ cu, $\eta_0 = 49{\cdot}04°$, $\eta_1 = 19{\cdot}58°$, $\eta_2 = -5{\cdot}20°$. We did not try using four phase shifts to improve the quality of the fit because at this level of accuracy we cannot be sure that spin–orbit coupling effects may be ignored any longer.

To calculate the specific resistivities of liquid mercury we can transform the $\eta_l(E_F)$ to a local form factor $\Gamma^{APW}(q, E_F)$ in the on Fermi sphere approximation (Devillers and de Vroomen 1971, Lee and Heine 1972) and then use $\Gamma^{APW}(q, E_F)$ as an approximate value for the matrix element in the well known Ziman formalism. For the structure factor we used the values of Halder and Wagner (1966). We take the usual expression

$$\rho^{calc}(\Gamma^{APW}(q, E_F)) \propto \frac{1}{r_F^2}\int_0^1 a(x)|\Gamma^{APW}(x, E_F)|^2 dx^3 \qquad (1)$$

with $x = q/2k_F$ and $r_F = k_F$. The result appears now to depend strongly on the value of E_F and we note a considerable overestimation of $\rho^{exp} = 96\,\mu\Omega$ cm (table 2).

As the backward scattering matrix elements are very large (varying between about $-0{\cdot}2$ and $+0{\cdot}2$ Ryd in the range $0{\cdot}6 \leq x \leq 1$) we expect considerable second order effects which may account for the observed discrepancies. Now, following a line of argument suggested by the work of Edwards (1962), we propose a semiphenomenological

Table 2. Calculated specific resistivity ρ^{calc} ($\mu\Omega$ cm) and m^* of liquid Hg at $T = 300$K with form factor Γ^{APW} and Γ^t as a function of Fermi energy. The latter are measured in crystal units (Devillers and de Vroomen 1971, Devillers 1972) for which the free electron value E_F^0 is 0·4245

	Γ^{APW}			Γ^t		
E_F	ρ^{calc}	m^*	$(m^*)^4\,\rho^{calc}$	ρ^{calc}	m^*	$(m^*)^4\,\rho^{calc}$
0·4245	489	0·662	94	66·6	1·113	102
0·35	350	0·728	98	67·3	1·014	72
0·30	298	0·756	97	80·4	0·998	80
0·25	267	0·775	97	109	0·966	95
0·15	224	0·809	97	238	0·818	106
0·10	207	0·826	96	314	0·701	76

correction factor $(m^*)^4$ to the calculated 'lowest order' specific resistivity. This correction can be thought of as follows.

We will use some identities, which are consistent with each other to second order: for the kinetic energy

$$E_{kin} = m^* v_F^2 = k_F^2/m^* \tag{2}$$

and

$$E_{kin} = \langle \psi^{(1)} \,|\, -\nabla^2 \,|\, \psi^{(1)} \rangle = \langle \psi^{(1)} \,|\, E_F - \Gamma \,|\, \psi^{(1)} \rangle \tag{3}$$

where $\psi^{(1)}$ is correct to first order in perturbation theory. Now for a moment we look at the solid. Then, in the nondegenerate case, it is a well known result that

$$E_{kin} = E_F - \Gamma_0 + 2\Sigma^{(2)} \tag{4}$$

with

$$\Sigma^{(2)} = \sum_{q_n}{}' \frac{|\,\Gamma q_n\,|^2}{|\,k_F + q_n\,|^2 - k_F^2}.$$

Combining (4) with the energy eigenvalue equation,

$$k_F^2 - E_F + \Gamma_0 - \Sigma^{(2)} = 0 \tag{5}$$

which is correct to second order, it follows that

$$E_{kin} = k_F^2 + \Sigma^{(2)} = k_F^2(1 + \Delta) \tag{6}$$

where we define

$$\Delta = (k_F^2 - E_F + \Gamma_0)/k_F^2. \tag{7}$$

Then from (2), (6) and (7) we obtain

$$m^* = (1 + \Delta)^{-1}. \tag{8}$$

Now we assume (2), (7) and (8) to be valid in the liquid too.

Equation (2) defines $v_F = k_F/m^*$ which is consistent with $v_F = \nabla_k E_k$. This results in a correction factor $(m^*)^2$ to ρ^{calc}. Further the $\Gamma^{APW}(q_n, E_F)$ (q_n for Hg lying in the backward scattering region) have been fitted to the splitting Δ_k on the Fermi surface at an energy dispersion relation k^2/m^* rather than at the free electron dispersion relation k^2; so $\Gamma^{APW}(q_n, E_F)$ is overestimating the Fourier transform V_{q_n} of the effective pseudopotential by a factor $1/m^*$ (Weaire 1967, Heine and Weaire 1970). This leads to an additional correction factor $(m^*)^2$.

The m^*, defined by (7) and (8), and the specific resistivity corrected by $(m^*)^4$ have been listed in table 2. We note a splendid agreement with ρ^{exp} for $E_F = \frac{1}{3}E_F^0$ (the theoretical choice of E_F in first order). However the corrected resistivity is amazingly independent of E_F. In our opinion this is related to the fact, that for Hg the 'focus point radii' (Devillers 1972) for $l = 1$ and 2 are very close to the Wigner–Seitz radius.

Testing our $(m^*)^4$ correction on white tin (using $\Gamma^{APW}(q, E_F)$ of Devillers and de Vroomen 1971) we again find that for $E_F \simeq \frac{1}{3}E_F^0$ an original overestimation of about 30% is reduced to a few per cent. However for $E_F \simeq E_F^0$ the corrected value deviates from the experimental one.

It is interesting to calculate the resistivity with the APW-deduced phase shifts in a t matrix formalism (Evans *et al* 1971). But here we take a modified t matrix in that we use $(E_F^0)^{1/2}$ in the denominator of the scattering matrix element rather than $(E_F)^{1/2}$, for we think the mean kinetic energy of the electrons at the Fermi energy is given in lowest order by k_F^2 rather than by E_F. In doing so the modified t matrix reduces to Ziman's quasi-potential (Ziman 1964)

$$\Gamma^l(q, E_F) = -\frac{\frac{2}{3}E_F^0}{Z}\frac{2}{\pi}\sum(2l+1)\exp(i\eta_l)\sin\eta_l P_l(\cos\theta). \tag{9}$$

Putting this form factor in equation (1) yields $\rho^{calc}(\Gamma_l(E_F))$ (table 2). For the very same reasons as in finding ρ^{calc} from $\Gamma^{APW}(q, E_F)$ we apply a correction $(m^*)^4$ but taking now, for the analogue of (7), $\Delta = (k_F^2 - E_F - |\Gamma_0|)/k_F^2$ (table 2). It is very gratifying that $\rho^{calc}(\Gamma^l(E_F)) \simeq \rho^{calc}(\Gamma^{APW}(E_F))$ for $E_F \simeq \frac{1}{3}E_F^0$ and that approximately the same $m^* = 0{\cdot}81$ is found here as previously. Moreover these values of m^* agree with those of Weaire (1967).

Another quantity which can be calculated from our $\Gamma^{APW}(q, \frac{1}{3}E_F^0)$ is the volume derivative $D = (\Omega_{at}/\rho^{calc})(d\rho^{calc}/d\Omega_{at})$ at the melting point. Ziman (1966) has given an approximate expression

$$D \simeq 2 - \tfrac{4}{3}p \tag{10}$$

with

$$p = -\frac{\int_0^1 a(x)\Gamma(x)(d\Gamma(x)/dx)x^4dx}{\int_0^1 a(x)|\Gamma(x)|^2x^3\,dx}. \tag{11}$$

We note that m^* corrections drop out from p as well as some scaling of $a(x)$ or $\Gamma(x)$. So, as pointed out by Ziman, p is a sensitive measure for q_0, ie the node in $\Gamma(q)$ at about $x = 0{\cdot}9$. We have calculated D for the Animalu–Heine form factor ($D = 3{\cdot}1$) the Evans form factor ($D = -3{\cdot}9$) and our present form factor ($D = 6{\cdot}0$). This latter compares well with the experimental value $D = 8{\cdot}2 \pm 0{\cdot}3$.

Another experimental phenomenon is the rather sharp decrease in ρ on alloying with many other metals. As far as we can see we may expect this, on the basis of the present work, since the general argument advanced by Evans (1970) continues to hold. The replacing of Hg atoms with numerically large V_q (of the order of 0·1–0·2 Ryd) by solute atoms with V_q of the order of several 0·01 Ryd in the important region $0{\cdot}6 < q/2k_F < 1$ seems to be the essential feature.

One of us (WHY) is grateful for helpful remarks from Dr R Evans and Professor Sir Nevill Mott.

References

Allen P B and Lee M J G 1972 *Phys. Rev.* B **5** 3848–57
Animalu A O E and Heine V 1965 *Phil. Mag.* **12** 1249–70
Bogle T E, Coon J B and Grenier C G 1969 *Phys. Rev.* **177** 1122–32
Brandt G B and Rayne J A 1966 *Phys. Rev.* **148** 644–56
Devillers M A C 1972 *Solid St. Commun.* **11** 395–400 and erratum
Devillers M A C and de Vroomen A R 1971 *Solid St. Commun.* **9** 1939–44
Dixon A E and Datars W R 1968 *Phys. Rev.* **175** 928–37
Edwards S F 1962 *Proc. R. Soc.* A **267** 518
—— 1966 *The Properties of Liquid Metals* ed P D Adam, H A Davies and S G Epstein (London: Taylor and Francis) p 359
Evans R 1970 *J. Phys.* C: *Metal Phys. Suppl.* **2** S137–52
Evans R, Greenwood D A and Lloyd P 1971 *Phys. Lett.* **35** 57
Evans R, Greenwood D A, Lloyd P and Ziman J M 1969 *Phys. Lett.* **30A** 313–4
Halder N C and Wagner C N J 1966 *J. chem. Phys.* **45** 482–7
Heine V and Weaire D 1970 *Solid State Physics* vol 24, ed H Ehrenreich, F Seitz and D Turnbull (New York: Academic Press) p 249
Jones J C and Datars W R 1971 *J. Phys.* F: *Metals Phys.* **1** L56–7
Lee M J G and Heine V 1972 *Phys. Rev.* B **5** 3839–47
Naguchi S and Takeuchi T 1973 to be published
Poulsen R G and Datars W R 1971 *Phys. Rev.* B **4** 4202–15
Poulsen R G, Moss J S and Datars W R 1971 *Phys. Rev.* B **3** 3107–15
Takeuchi T 1971 *J. Phys. Soc. Japan* **30** 995–1006
Weaire D 1967 *Proc. Phys. Soc.* **92** 956
Ziman J M 1964 *Adv. Phys.* **13** 89
—— 1966 *The Properties of Liquid Metals* ed P D Adams, H A Davies and S G Epstein (London: Taylor and Francis) p 551

APPENDIX C.

The Fermi surface of mercury from an APW interpolation.

(reprinted from J. Phys. F: Metal Physics, 1974, vol. 4)

THE FERMI SURFACE OF MERCURY FROM AN APW INTERPOLATION

M.A.C. Devillers and A.R. de Vroomen

Fysisch Laboratorium, Katholieke Universiteit Nijmegen,

The Netherlands

ABSTRACT

Muffin tin parameters are used in the APW scheme to fit recent accurate de Haas-van Alphen data. The interpolated Fermi surface is in good agreement with magneto acoustic and magneto resistance data. A form factor, decuded from the fitted muffin tin parameters, is proposed which yields, when used in Ziman's theoretical expressions for the specific resistivity of the liquid and its volume derivative, excellent agreement with the experimental values.

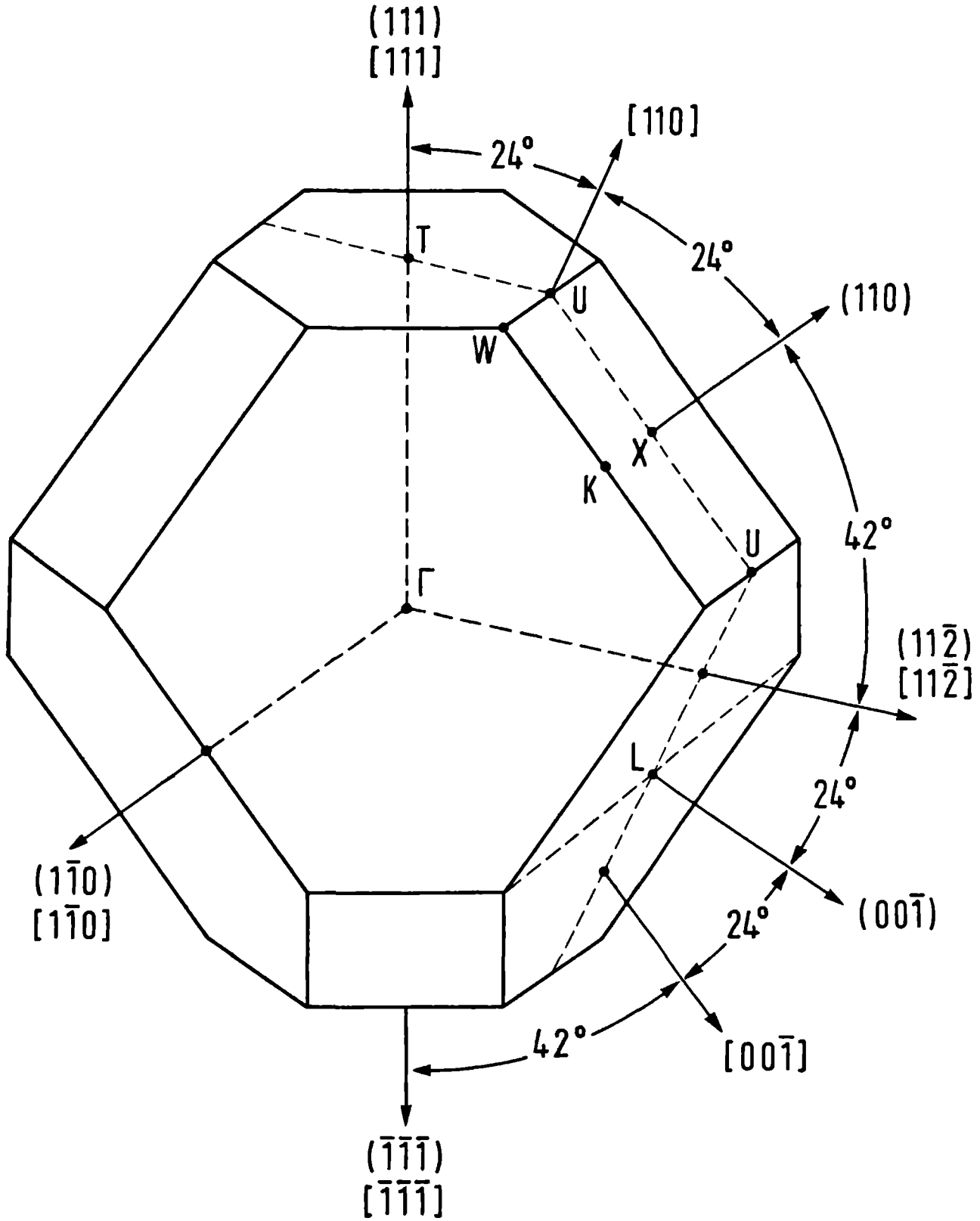

Figure 1 : Brillouin zone of mercury. Nomenclature after Bogle et al (1969).

1. Introduction

In the past several aut hors (Brandt et al 1966, Bogle et al 1969, Jones et al 1971) tried to describe the experimental known geometry and other related properties of the Fermi surface (FS) of mercury in terms of local pseudo potential form factors. In their results as well as in the work of others on the form factor of mercury (see for example Evans 1970, Takeuchi 1971) an ambiguity appeared as to the sign of the Fourier transforms of the pseudo potential in the backward scattering region $q \approx 2\ k_F$, k_F being the radius of the free electron Fermi sp here. The resolution of this ambiguity has been reported in a former paper (Devillers et al 1973) where the APW scheme has been used to deduce the scattering phase shifts $\eta_1(E_F)$ from accurate de Haas van Alphen (dHvA) measurements of Poulsen et al (1971).

In this paper we will give a more detailed picture of the FS of mercury, especially we will concentrate on those details which are not recognized earlier and we will compare the calculated FS calipers with magneto acoustic ones of Bogle et al (1967). Further we report the numerical results of several muffin tin parameters; $\eta_1(E_F)$, Friedelsum $Z_F(E_F)$ and a phase shift decuded form factor $\Gamma^{APW}(q,E_F)$. The latter will be discussed, especially with regard to second order effects as mentioned in Devillers et al (1973).

Table 1

Phaseshifts η_l, Friedelsum Z_F and Δ_{rms} [a)] on five dHvA areas (in per cent) as a function of E_F.

E_F	η_o	η_1	η_2	Z_F	Δ_{rms}
.4245	.441	.120	-.199	-.126	2.2
.35	.678	.258	-.130	.511	1.6
.30	.856	.342	-.091	.909	1.5
.25	1.049	.417	-.059	1.275	1.6
.15	1.512	.468	-.016	1.804	2.7
.10	1.806	.388	-.0056	1.91	3.5

$$^{a}\Delta_{rms} \equiv 10^2 \left\{ \frac{1}{5} \sum_{i=1}^{5} (A^i_{calc}/A^i_{exp} - 1)^2 \right\}^{\frac{1}{2}}$$

2. Calculation and results

The calculation has been performed in a simular way as was done for white tin (Devillers et al 1969, Devillers et al 1971), but now we are fitting three logarithmic derivatives $\alpha_l(E_F,R)$ in a relative least squares sense to experimental dHvA areas rather than to semi calipers of the FS in an absolute least squares sense. Although the five dHvA areas $\alpha(1\bar{1}0)$, τ, τ^1, β and $\eta(111)$ (notation of Poulsen et al 1971), chosen as to represent the FS, are differing by two orders of magnitude, we have given them equal weighting factors. About fifty APW's were taken into account, which seems to be sufficient for the obtained quality of fit. The same is true as regards the truncation of the l-summation at $l_{max} = 5$. As usually the muffin tin radius R was taken as the half nearest neighbour distance $R_I = 0.5$ c.u. (crystal units (c.u., see Devillers et al 1971) are used throughout; the lattice constant a = 2.9863 Å; conversion factor for energies to Ry: $.8068^{-1}$). We did not include spin orbit coupling, because we suppose this to be of minor influence for the shape of the FS, again within the limits of the obtained quality of fit.

The resulting phase shifts are given in table 1 as a function of E_F as well as their Friedel sum $Z_F(E_F)$ and the r.m.s. deviation. At the energy $E_F = 0.30$ c.u. the

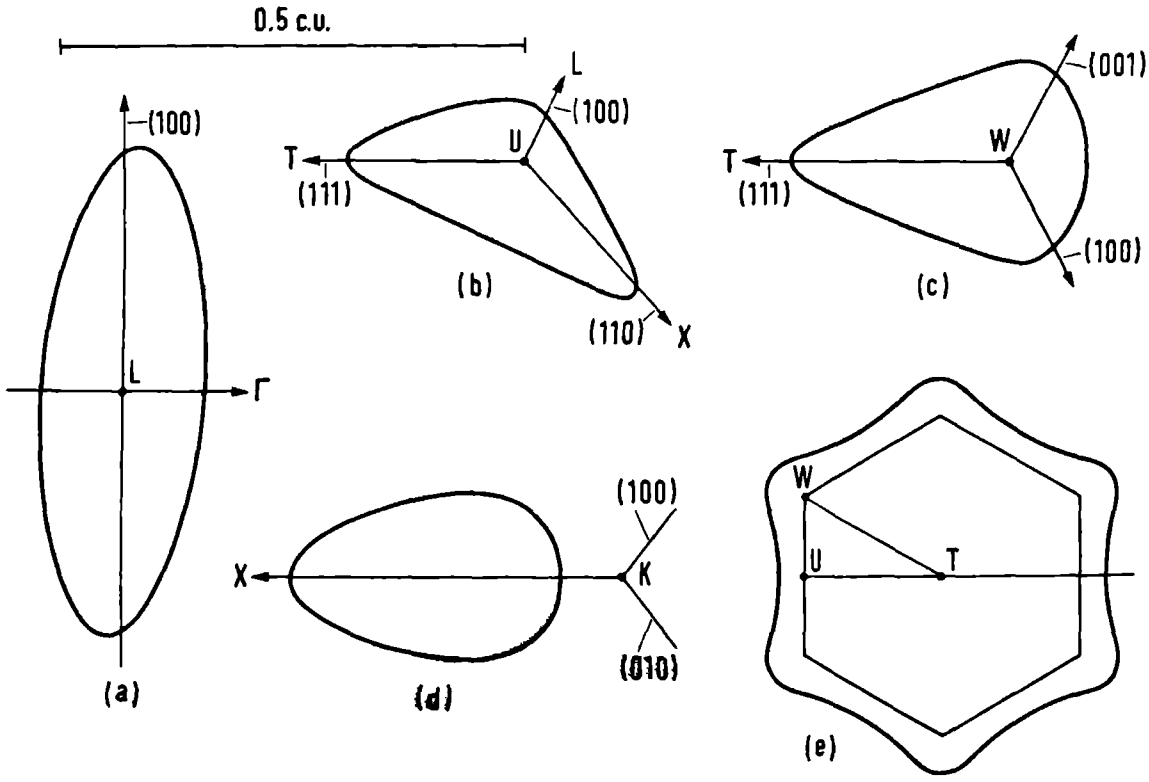

Figure 2 : APW interpolated dHvA cross sections of the Fermi surface of mercury: $\alpha(1\bar{1}0)$ (figure 2a), τ (figure 2b), τ' (figure 2c), β (figure 2d) and $\eta(111)$ (figure 2e). Figure 2d and 2e have been enlarged by factors 5 and .5 respectively with respect to the other cross sections.

deviation of the calculated areas $\alpha(110)$, τ, τ^1 and β to the experimental ones is less than 1%, the $\eta(111)$ area deviates 3% (table 2). These calculated extremal cross sections are shown in figure 2. (see also figure 1).

Figure 2a shows clearly an asymmetry of the electron disk with respect to the (100)Brillouin zone face: the normal to the extremal cross sectional plane is shifted about 3° from the (100) direction towards the (111) direction. Experimental support for this asymmetry is found in the cyclotron resonance measurements of Poulsen et al (1971). Further support is found in the dHvA branch α_3(Poulsen 1971, figure 5), which is symmetric around 26° from (111) direction rather than around 24°. The lens is not a figure of revolution around the short axis. This is shown by $\alpha(111)$ (table 2). If there were no asymmetry then $\alpha(111) \approx \alpha(1\bar{1}0)/\cos(24^\circ) = .076$ c.u. The τ-orbit (figure 2b) shows some asymmetry too i.e. the Fermi velocity v_F in the (100) and (110) Brillouin zone faces is not parallel to the UL- and UX-direction respectively. All those slight asymmetries have consequencies for the interpretation of dHvA and magneto acoustic measurements. Not all of them we have re-analysed (see various notes to table 3).

The calculated calipers are in good agreement with the magneto acoustic measurements of Bogle et al (1969) (table 3). One notes two large discrepancies between

Table 2.

Comparison with dHvA experiments

	A_{exp} [a]	exp.error (%)	$(A^{calc} - A_{exp})/A_{exp}$ x100
$\alpha(1\bar{1}0)$	.0699	.3	+ .8
τ	.0338	.7	- .3
τ'	.0444	.5	+ .9
β	.00159	.7	.0
$\eta(111)$	.472	1.4	-3.1
$\alpha(111)$	.0815	.4	+1.9
T-nek	(.0420)[b]		(.0333)[c]

[a] Poulsen et al (1971)

[b] Poulsen doubts his interpretation of this dHvA-branch

[c] Calculated value A^{calc}.

experimental and calculated calipers in table 3: k_{in}^{XU} and c_{τ}^{LU}. For the disagreement in k_{in}^{XU} we have no satisfying explanation; of course the asymmetry of the τ-orbit (X is an inversion point and XK is a mirror line) causes that one does measure between points with v_F // XU, but it is difficult to see from figure 2b that this accounts fully for the observed discrepancy. Concerning the c_{τ}^{LU} experimental value : here the discrepancy with our calculation is such that, taking into account the consistency of the τ-orbit with all other experimental data, it seems inevitable to conclude that the interpretation of the experiment is wrong. As a consequence the value of k_{out}^{LU} quoted by Bogle (1969) is wrong too by the amount $\Delta k = .035$ c.u.

3. APW form factor

With the "on the Fermi sphere" approximation the APW matrix elements can be transformed easily to a form factor $\Gamma^{APW}(q,E_F)$ (Devillers et al 1971). As reported in an earlier paper (Devillers et al 1973) one can use $\Gamma^{APW}(q,E_F)$ to compute the specific resistivity of liquid mercury as well as the volume derivative of the resistivity. Figure 3 shows $\Gamma^{APW}(q,E_F)$ for some values of E_F. For comparison we show the theoretical form factors of Animalu and Evans too (Evans 1970), as well as some

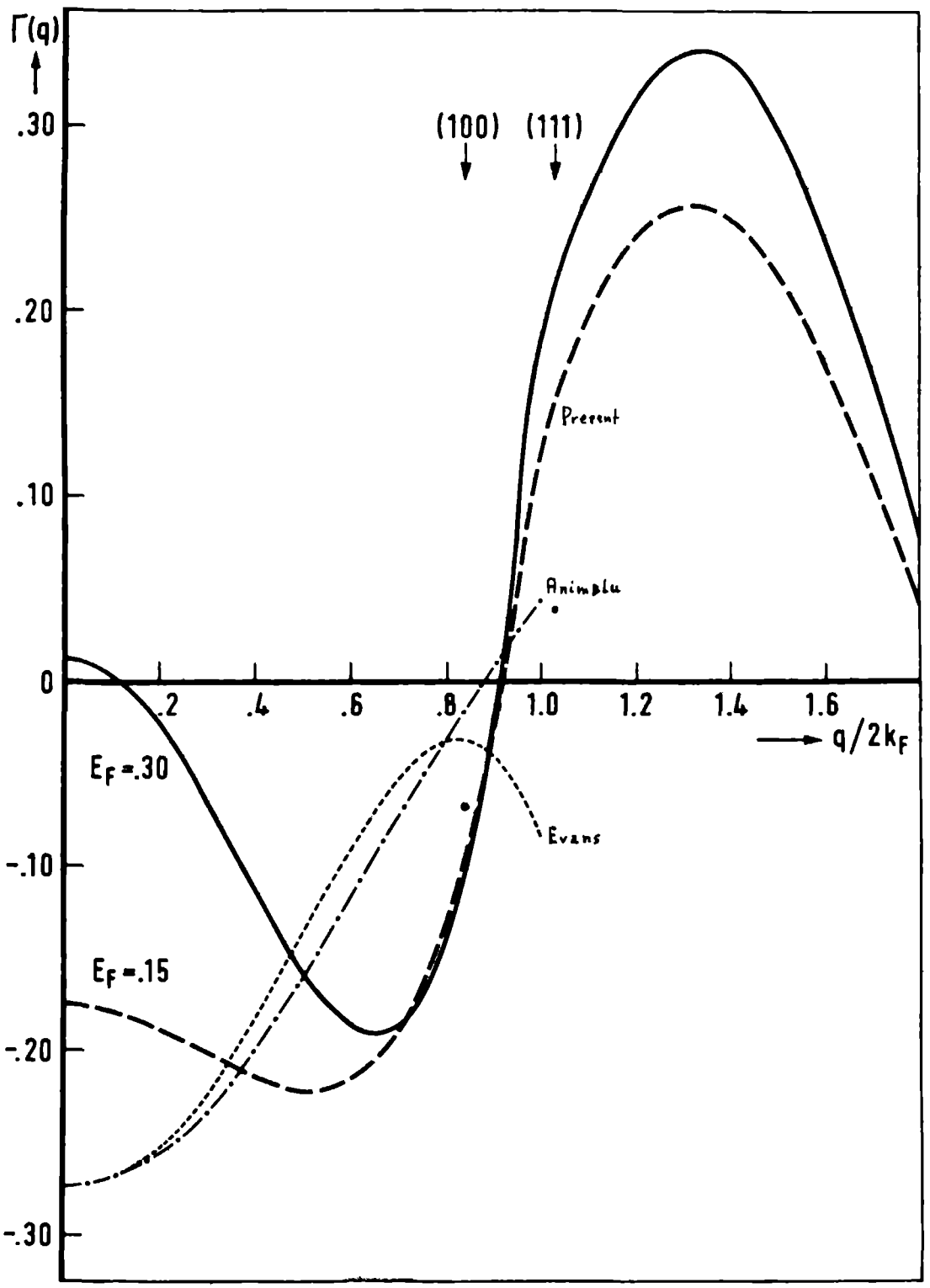

Figure 3 : Form factor $\Gamma^{APW}(q,E_F)$ (this work), V(q) of Animalu and Heine and V(q) of Evans (1970) respectively as a function of $q/2K_F$. The heavy dots are values quoted by Jones and Datars (1971).

fitted $V(q_n)$ of Jones and Datars (1971). Our form factor has apparently stronger backward scattering matrix elements, for a large part caused by the 1-2 contribution. This causes considerable second order effects which not only gives rise to an effective band mass m^* (Devillers et al 1973), but makes it difficult too to compare our $\Gamma^{APW}(q_n, E_F)$ with the fitted $V(q_n)$, which include implicitly the second order effects.

Because the APW determinant in the fit procedure is solved exactly (within the limits of required numerical convergence of course) the numerical values of the APW matrix elements possess a selfconsistency to all orders. It is reasonable to assume that contributions, which may be seen as third or higher order can be ignored in our problem. So if we assume now the "on the Fermi sphere" approximation to be a good approximation to the band structure problem we may assume too that the values of $\Gamma^{APW}(q, E_F)$ for $q \gtrsim 2k_F$ are consistent automatically with the second order energy eigenvalue equation on the diagonal. And this may be an important note, because it is not clear wether in model potential calculations this nevessary consistency is assured when poeple force $V(o) = -\frac{2}{3} E_F^o$, which is a <u>first</u> order perturbation condition. To use Γ^{APW} in nearly free electron theories the only thing to do seems to be the introduction of some appropriate m^* correction (Devillers et al 1973).

Another point, we mention in respect with the re-

liability of Γ^{APW}, concerns the higher l-values ($l \geq 3$) and spin orbit coupling, which we did not include explicitly in our fitting procedure. However, one may expect these contributions to be included effectively in the three parameters used, in other words $\Gamma^{APW}(q, E_F)$ is expected to alter very little if we were including higher l terms or a spin orbit coupling term.

4. Conclusion

We have given a rather accurate description of the FS of solid mercury in terms of phase shifts of the muffin tin potential. The calculated extremal cross sections and calipers of the FS are in good agreement with the available experimental data. We have found a number of slight asymmetries in the shape of the FS, which were not recognized earlier. An experimental re-investigation of the FS with the aid of dHvA or radio frequency size effect experiments might be worthwhile to check the predicted asymmetries.

Finally we propose an atomic form factor $\Gamma^{APW}(q, \frac{1}{3}E_F^o)$ which may be used to calculate properties like the specific resistivity of liquid mercury and its volume derivative. The specific resistivity, calculated with $\Gamma^{APW}(q, \frac{1}{3}E_F^o)$ and at 300°K, is 97 $\mu\Omega$cm, whereas the experimental value is 96 $\mu\Omega$cm. For more details of this application of Γ^{APW} the interested reader is refered to a former paper (Devillers et al (1973).

Table 3

Comparison with magneto acoustic calipers

(unit .001 c.u.)

Caliper[a]	Exp.[a]	APW	Caliper	Exp.	APW
$k_{lens}^{L-\Gamma}$	84 ± 2	87	k_{out}^{L-U}	542 ± 15[e]	582
k_{lens}^{L-U}	256 ± 5	263[b]	k_{out}^{T-U}	366 ± 10[f]	352
k_{lens}^{L-W}	304 ± 8	288	k_{out}^{X-U}	364 ± 10[g]	387
k_{in}^{L-U}	428 ± 10	439	k_{out}^{T-W}	428 ± 10	427
k_{in}^{X-U}	142 ± 5	118	c_{τ}^{L-U}	115 ± 10[e]	149
k_{in}^{T-U}		104[c]	$c_{\tau'}^{(111)}$	226 ± 20	219
k_{in}^{T-W}		104[c]	Δk_{β}^{X-K}	62 ± 10	58
k_{in}^{X-K}		100	k_{out}^{X-K}		158
$k_{in}^{T-W} + K_{in}^{X-K}$	≈ 190[d]	204			

Table 3 (continued)

[a] From Bogle et al 1969

[b] Projection of lens on LU-direction.

[c] T-opening appears to be circular to within .001 c.u.

[d] Estimated by Poulsen et al 1971 from de Haas-van Alphen cut-off angles and angular ranges of "magneto-resistance open orbits".

[e] Wrong interpretation of experiment ? See text.

[f] Note shape of η-orbit in Figure 2e; experiment measures projection of $\eta(111)$-orbit on TU-direction (=.375 c.u.), rather than k_{out}^{T-U}.

[g] Measures indirectly from ϵ_1 orbit, suffers from symmetric interpretation of lens; correction of 3^{o} would remove discrepance.

References

Bogle, T.E., Coon, J.B., and Grenier, C.G., 1969, Phys.Rev., 177, 1122-32

Brandt, G.B., and Rayne, J.A., 1966, Phys.Rev., 148, 644-56.

Devillers, M.A.C., and de Vroomen,A.R., 1969, Phys.Letters, 30A, 159-61.

Devillers, M.A.C., and de Vroomen,A.R., 1971, Sol.Stat.Comm., 9, 1939-44.

Devillers, M.A.C., Young,W.H., and de Vroomen,A.R., 1973, to be published

Evans,R., 1970, J.Phys.C: Metal Phys.Suppl., 2, S137-52.

Jones,J.C., and Datars,W.R., 1971,J.Phys.F Metal Phys., 1, L56-7.

Poulsen,R.G., Moss,J.S., and Datars,W.R., 1971, Phys.Rev.B, 3, 3107-15.

Poulsen,R.G., and Datars,W.R., 1971,Phys.Rev.B 4, 4202-15.

Takeuchi,T., 1971, J.Phys.Soc.Japan, 30, 995-1006.

SUMMARY

The muffin tin potential model has been used in the past to develop several band structure schemes like APW, KKR and KKRZ. The ab initio construction of the crystal muffin tin potential is a hard task however. On the other hand, the muffin tin potential enters in the band structure theory as logarithmic derivatives, α_l (E_F,R), of the radial part of the "atomic" solutions of a single muffin tin potential at the inscribed sphere radius R, or, equivalently, as the phase shifts η_l (E_F) of such a single muffin tin potential. And it is noted that, at the Fermi energy E_F, these quantities are constants. So they can be used as parameters to describe Fermi surfaces, when for example the latter have been measured by de Haas-van Alphen or radio frequency size effects. It is also noted that they are expected to be more adequate than the Fourier transforms of some local pseudopotential. These ideas form the basis for our thesis work.

It turns out that indeed the α_l are very suitable for interpolation of Fermi surface data. This has been shown for the examples white tin, copper and mercury respectively.

Further, it is investigated whether the parameters obtained have any physical significance other than for Fermi surface interpolation purposes. An application of them has been found in using them in a theoretical expression for the specific resistivity (and its volume derivative) of liquid metals.

From our work an apparent E_F-ambiguity has been found, the reason for which has been traced back via arguments from local pseudopotential theory. Some consequences of the E_F-ambiguity for the fitted parameters and the relationship of them with the "focus point" parameters of Andersen have been analysed.

Also the relations between Bloch theory of crystalline metals and scattering theory of densily packed scattering potentials have been clarified considerably. As to the present state of scattering theory in metals we advance a modified theory which accounts better for the kinematics of the conduction electrons and at the same time gives rise to the incorporation of second order effects in band structure theory in a very simple way.

SAMENVATTING

Het muffin tin potentiaal model is in het verleden gebruikt voor de ontwikkeling van bandstructuur schema's als APW,KKR enKKRZ. De ab initio constructie van een numeriek nauwkeurige kristal muffin tin potentiaal is echter een moeilijke opgave. Anderzijds is het zo, dat in de uiteindelijke determinant uitdrukking voor de energie-eigenwaarde van een Bloch electron de muffin tin potentiaal impliciet verschijnt in de logarithmische afgeleiden, $\alpha_l(E_F,R)$, van het radiele deel van de "atomaire" oplossingen van een enkele muffin tin potentiaal, of, equivalent, als phase shifts $\eta_l(E_F)$ van zo'n enkele muffin tin potentiaal. En we merken op, dat, voor gegeven Fermi energie, deze grootheden constanten zijn; met als gevolg dat ze als parameters gebruikt kunnen worden voor de beschrijving van een experimenteel bepaald Fermi oppervlak. Ook merken we op, dat naar verwachting de muffin tin parameters meer geeigend zijn voor de parametrizatie van Fermi oppervlak gegevens dan de vooral vroeger vaak gebruikte Fourier getransformeerde van een lokale pseudo potentiaal. Deze ideeen vormen de basis van ons promotie onderzoek.

Uit ons onderzoek blijkt, dat de α_l uitmuntend geschikt zijn voor interpolatie van ook topologisch-geometrisch ingewikkelde Fermi-oppervlakken. Als voorbeelden zullen we respectievelijk de interpolatie van het Fermi-oppervlak van wit tin, die van koper en die van kwik gebruiken.

Verder hebben we onderzocht of de verkregen parameters een zodanige physische betekenis hebben, dat ze ook voor andere dan interpolatie doeleinden gebruikt kunnen worden. Een toepassing hebben we gevonden door ze via de "on the Fermi sphere approximation" te gebruiken in de

theoretische uitdrukking voor de specifieke weerstand (en diens volume afgeleide) van vloeibare metalen.

Uit de resultaten van ons onderzoek blijkt verder een duidelijke E_F-ambigiteit. De reden hiervan hebben we opgespoord met gebruikmaking van argumenten, ontleend aan de theorie voor lokale pseudo potentialen. Sommige konsekwenties van de E_F-ambigiteit voor de muffin tin parameters, alsmede hun relatie met de "focus-point" parameters van Andersen, hebben we geanalyseerd.

Ook de relaties tussen Bloch theorie van kristallijne metalen en strooiingstheorie voor dichtgepakte strooiende potentialen zijn aanzienlijk verhelderd. Wat betreft de huidige stand van zaken in strooiingstheorie voor metalen stellen we een gemodificeerde theorie voor, welke de kinematica van de geleidingselectronen beter in rekening brengt en tegelijkertijd voert tot het op een zeer eenvoudige manier in rekening brengen van tweede orde effecten in bandstructuurtheorie.

Curriculum vitae

Geboren: 3 oktober 1937 te Wouw.

In 1956 werd het diploma Middelbare Landbouwschool te Roosendaal behaald; van 1956 tot 1961 werkzaam als medebedrijfsleider op agrarisch bedrijf; in 1961 werd het diploma Staatsexamen HBS-B behaald en in 1968 het doctoraal natuurkunde aan de Katholieke Universiteit te Nijmegen.

Van 1968 tot 1973 werkzaam als wetenschappelijk medewerker in de groep experimentele natuurkunde I onder leiding van Professor A. R. de Vroomen en sinds januari 1974 als Senior Research Associate aan de University of East Anglia, Norwich, Engeland.

Nijmegen, mei 1974 M. A. C. Devillers

STELLINGEN

I

Er zijn duidelijke aanwijzingen, dat Ziman's "zwakke storing" uitdrukking voor de specifieke weerstand van vloeibare metalen tot in tweede orde correct gemaakt kan worden door deze met een $(m^*)^4$ correctie-factor te vermenigvuldigen.

Dit proefschrift.

II

De verschillen van de theoretische waarden van de specifieke weerstand van vloeibaar zink en vloeibaar cadmium ten opzichte van hun respectieve experimentele waarden kunnen teniet gedaan worden door een geschikt gedefinieerde tweede orde correctie-factor.

A.J.Greenfield en N.Wiser,1973,
J.Phys.F: Metal Phys., 3, 1397.

III

De t-matrix voor elastische verstrooiing kan geschreven worden als het product van een factor, die alleen van de kinematica van het inkomende deeltje afhangt,en van een factor, die alleen van de verstrooiende eigenschappen van de target afhangt.Dit feit wordt niet voldoende benadrukt in vele handboeken.

bv. E.Merzbacher,Quantum Mechanics,
John Wiley & Sons, Inc.,New York
1961, chapter 12, 21.

IV

De eerste Born benadering wordt niet noodzakelijk ongeldig, wanneer een partiele phase shift van de grootte orde van een radiaal is.

V

Voor de beschrijving van thermische positronen in metalen kan het muffin tin model een nuttige benadering zijn voor de positron-metaal interactie potentiaal.

VI

De lage energie limiet voor de partiele phase shifts in muffin tin metalen impliceert niet noodzakelijkerwijs, dat de corresponderende logarithmische afgeleiden de "empty potential" waarden aannemen.

Dit proefschrift.

VII

Het bestaan van som-banen in radiofrequente size effect experimenten geeft de mogelijkheid om afstanden tussen punten op het Fermi oppervlak te meten, die in die experimenten niet rechtstreeks als fundamentele calipers gemeten kunnen worden.

VIII

Huidige methoden voor de berekening van interatomaire krachten in metalen via de Born-Green of de Percus-Yevick theorie zijn in principe incorrect.

M.A.C. Devillers

Nijmegen, mei 1974.